Journal of Computational Physics: X 8 (2020) 100078

Contents lists available at ScienceDirect

Journal of Computational Physics: X

www.elsevier.com/locate/jcpx

Euler-Lagrange modelling of dilute particle-laden flows with arbitrary particle-size to mesh-spacing ratio

Fabien Evrard *, Fabian Denner, Berend van Wachem

Lehrstuhl für Mechanische Verfahrenstechnik, Otto-von-Guericke-Universität Magdeburg, Universitätsplatz 2, 39106 Magdeburg, Germany

ARTICLE INFO

Article history:
Received 24 October 2019
Received in revised form 26 June 2020
Accepted 30 September 2020
Available online 6 October 2020

Keywords:
Euler-Lagrange
Dilute particle-laden flow
Velocity correction
Source term regularisation

ABSTRACT

This paper addresses the two-way coupled Euler-Lagrange modelling of dilute particle-laden flows, with arbitrary particle-size to mesh-spacing ratio. Two-way coupled Euler-Lagrange methods classically require particles to be much smaller than the computational mesh cells for them to be accurately tracked. Particles that do not satisfy this requirement can be considered by introducing a source term regularisation operator that typically consists in convoluting the point-wise particle momentum sources with a smooth kernel. Particles that are larger than the mesh cells, however, generate a significant local flow disturbance, which, in turn, results in poor estimates of the fluid forces acting on them.
To circumvent this issue, this paper proposes a new framework to recover the local undisturbed velocity at the location of a given particle, that is the local flow velocity from which the disturbance due to the presence of the particle is subtracted. It relies upon the solution of the Stokes flow through a regularised momentum source and is extended to finite Reynolds numbers based on the Oseen flow solution. Owing to the polynomial nature of the regularisation kernel considered in this paper, a correction for the averaged local flow disturbance can be analytically derived, allowing to filter out scales of the flow motion that are smaller than the particle, which should not be taken into account to compute the interaction/drag forces acting on the particle. The proposed correction scheme is applied to the simulation of a particle settling under the influence of gravity, for varying particle-size to mesh-spacing ratios and varying Reynolds numbers. The method is shown to nearly eliminate any impact of the underlying mesh resolution on the modelling of a particle's trajectory. Finally, optimal values for the scale of the regularisation kernel are provided and their impact on the flow is discussed.

© 2020 The Author(s). Published by Elsevier Inc. This is an open access article under the CC BY-NC-ND license (http://creativecommons.org/licenses/by-nc-nd/4.0/).

1. Introduction

Particle-laden flows are ubiquitous in nature as well as in industrial applications. Nevertheless, our understanding of the collective dynamics of particles in a flow remains partial, and colossal amounts of man-hours have been spent with the aim to improve it. Alongside its experimental counterpart, the study of particle-laden flows by means of numerical modelling has grown in importance over the past decades, due to the steady increase of computing resources and the development of faster and more accurate numerical methods. The family of numerical methods available for the modelling of particle-laden flows ranges from "particle-resolved" Immersed-Boundary (IB) methods, where the flow around each individual particle is

* Corresponding author.
E-mail address: fabien.evrard@ovgu.de (F. Evrard).

https://doi.org/10.1016/j.jcpx.2020.100078
2590-0552/© 2020 The Author(s). Published by Elsevier Inc. This is an open access article under the CC BY-NC-ND license (http://creativecommons.org/licenses/by-nc-nd/4.0/).

resolved on the computational mesh [1,2], to fully Eulerian approaches, where both phases are considered as a continuum [3,4]. Between these two approaches lies the Euler-Lagrange approach, where the fluid phase is considered as a continuum, but the individual trajectories of the particles are resolved. Euler-Lagrange (EL) point-particle methods constitute an accurate, straightforward, and cost-effective way to model flows that are laden with up to a few million particles [5–8]. In EL approaches, the flow of the carrying fluid phase is solved within a classical Eulerian framework, while the particles, assimilated to Lagrangian point-masses, are tracked based on the underlying flow field. The forces acting on the particles, *e.g.* drag, are typically estimated using semi-empirical models. Various levels of coupling between the fluid and the particulate phases can be considered, each associated with different volume-fraction regimes [7,9,10]. For dilute particle-laden flows with very low particle volume fraction, one-way coupling may be considered. In such cases, the transfer of momentum from the Lagrangian particles to the Eulerian fluid phase is neglected, meaning that the flow is unaffected by the presence of the particles. At particle volume fraction as low as 10^{-5}, however, this momentum transfer cannot be neglected anymore, and the flow is therefore impacted by the particles through a source term contribution in the governing momentum equations [9,11]. This is referred to as two-way coupling. Finally, when the local fraction of volume occupied by the particles is a few orders of magnitude larger than this limit, *i.e.* in dense particle-laden flows, then this local volume fraction needs to be taken into consideration in the governing flow equations to account for the narrowing of the fluid flow domain, leading to an additional component of coupling between the continuous phase and the particle phase [3].

This paper addresses the two-way coupled EL modelling of dilute particle-laden flows, that is when: (a) the transfer of momentum from the Lagrangian phase to the Eulerian phase is accounted for in the governing momentum equations; and (b) the local fraction of volume occupied by the particles may be considered negligible, and hence does not appear in the governing equations for the continuous phase. One major challenge that arises, when considering such an approach, is the estimation of the *undisturbed* flow velocity at the location of the Lagrangian particles [8,12–14]. The undisturbed velocity is defined as the local velocity as if the particle under consideration is taken out of the flow, *i.e.* has no influence on it. It is a quantity required to estimate the interaction between the phases, such as the drag force, using semi-empirical models. In the context of the two-way coupled EL modelling of particle-laden flows, the momentum that is fed back to the fluid by a given particle generates a local flow disturbance. This means that the flow velocity available on the Eulerian mesh is not representative of the undisturbed velocity, but rather corresponds to a *disturbed* flow velocity. Drag – and therefore the motion of the particle – is, as a result, predicted with an error as the *disturbed* flow velocity is used to evaluate it. This feature of the two-way coupled EL method is well illustrated by considering the case of a single, isolated particle falling in a quiescent fluid under the influence of gravity. In this configuration, the undisturbed velocity is equal to zero throughout the fall of the particle, since removing the particle from the flow would leave the initially quiescent fluid unperturbed. In the framework of the two-way coupled EL method, however, the momentum that the tracked particle feeds back to the fluid generates a local flow disturbance. When interpolating the fluid velocity to the location of the particle, this manifests itself by a finite fluid velocity component in the direction of motion of the particle. Using this velocity to estimate the drag force acting on the particle results in the underestimation of this force. In turn, the terminal velocity that is predicted by the two-way coupled EL framework is overestimated compared to the analytical solution.

From a numerical viewpoint, the transfer of momentum between the particles and the fluid in the EL framework is typically addressed using the particle-source-in-cell (PSI-CELL or PSIC) model of Crowe et al. [15]. In the framework of the PSIC-EL method, the magnitude of the velocity disturbance induced by the momentum fed back to the fluid by a given particle can be shown to grow proportionally with the ratio d_p/h [13,16], where d_p is the particle diameter, and h is the mesh spacing. In turn, this means that the error in the estimation of the drag force acting on a particle also grows proportionally with d_p/h. As a result, the tracked particles are required to be much smaller than the mesh cells (*i.e.* $d_\mathrm{p} \ll h$) in order to keep these errors small. The PSIC-EL method has been widely used over the past decades to simulate particle-laden flows (see *e.g.* [5,6,17]). The requirement $d_\mathrm{p} \ll h$, however, limits the range of particulate flows that can accurately be modelled with this approach, since high mesh resolutions may sometimes be required in order to resolve all relevant flow scales, account for complex geometries, etc., resulting in particles that are of a similar size as, or larger than, the computational cells. Recent work has been dedicated to the extension of the PSIC-EL method to particles that do not satisfy $d_\mathrm{p} \ll h$, addressing the momentum transfer by means of convolution with smooth kernels of arbitrary scale [18–20]. These approaches mitigate the errors due to the two-way coupling between the fluid and the particles, since the magnitude of the flow disturbance induced by the momentum transfer reaches a plateau as d_p/h increases, instead of growing proportionally with this ratio. The value of this plateau directly relates to the length-scale of the regularisation kernel. Spreading the transferred momentum over a wider region results in smaller errors. For a given regularisation length-scale, however, further mitigating the errors in the estimation of the drag force requires a strategy to recover the undisturbed velocity from the disturbed velocity field available on the Eulerian mesh, as well as the other parameters of the flow. The recovery of the undisturbed velocity at the location of a particle tracked in the two-way coupled EL framework is addressed in [12–14,21,22]. Gualtieri et al. [21] propose to consider the particle-induced forces acting on the flow to have diffused over a short period of time, thus allowing to evaluate the disturbance flow produced by the particles in a closed form. Their study exhibits promising results, but is limited to small Reynolds numbers and a point-wise velocity correction. Horwitz and Mani [13,22] propose to recover the undisturbed flow velocity with a correction function whose coefficients are fitted based on the results of many numerical simulations, first in the Stokes limit [22], and then in the finite Reynolds number

regime [13]. This produces very good results but is evidently dependent on the type of solver that is used, and therefore lacks generality. Ireland and Desjardins [12] propose to subtract the fictitious filtered Stokes flow around the spherical particle from the local flow. Although this approach sometimes yields good results, the flow disturbance resulting from the momentum contribution of a particle does not locally converge to the equivalent Stokes flow around the spherical particle, owing to the very nature of the momentum transfer in EL methods. An approach for the recovery of the undisturbed velocity that aims to allow for arbitrary ratios between the regularisation scale and the particle diameter, and aims to exhibit a convergent behaviour as the mesh is refined, should be based on the flow through a regularised momentum source, as opposed to the filtered flow around a rigid particle. Such an approach was adopted by Balachandar et al. [14], and shown to yield good results for the case of a falling particle. Their scheme corrects the point-wise flow velocity interpolated to the centre of the particle. However, in the context of a flow that may exhibit scales that are smaller than the particle, it is physically more correct to consider an averaged fluid velocity integrated over a volume whose length-scale is similar to that of the particle, since the scales of the flow that are similar or larger than the particle drive the flow-induced particle motion [23,24]. Additionally, as shown by Maxey and Patel [23], such an averaged form of the velocity allows for a consistent balance between the energy released by a particle and the viscous dissipation in the fluid. So, although recovering the undisturbed fluid velocity at the location of a particle is a very timely topic and a topic for which some research has been conducted, there is not yet a generally applicable approach.

In this paper, we propose a novel approach to recover the locally averaged undisturbed flow velocity, building on our previous work [19] as well as the work of Balachandar et al. [14]. While our previous work addresses in detail the geometric filtering of the governing equations/source term regularisation for the two-way coupled EL modelling of particle-laden flows [19], the current article focuses on the recovery of the undisturbed flow velocity in such a context. The consideration of the locally averaged flow velocity, as opposed to the point-wise velocity interpolated to the centre of the particle, rests on physical grounds but also allows for a consistent energy balance between the Lagrangian particles and the fluid [23]. Our choice of regularisation kernel [19] differs from that made in other works, and enables us to analytically derive the correction for the averaged undisturbed velocity. The novelty of the work presented in this paper is twofold: (a) we propose the first undisturbed velocity recovery scheme that is derived for the Wendland regularisation kernel (as opposed to the Gaussian kernel considered in [12,14], for instance); and (b) this is the first occurrence of such a scheme applied to the locally averaged velocity (as opposed to the point-wise velocity interpolated to the centre of the particle). Due to the polynomial nature of the Wendland kernel, the expressions derived in this paper are analytical, polynomial functions too. Moreover, our approach can be extended to other types of averaging operators and can, conceptually, be derived for any velocity interpolation scheme. The current work is limited to an incompressible carrier phase. The extension of the volume-filtered EL method [18–20] to a compressible carrier phase is still a very new subject of research [25], and lies outside the scope of this paper.

This paper is organised in the following manner: Section 2 presents the governing equations for the Eulerian and Lagrangian phases. The regularisation of the particle momentum sources is discussed in Section 3, where we also present and justify our choice of regularisation function. The correction for the locally averaged particle-induced flow disturbance is derived, discussed, and tested in Section 4. Finally, Section 5 summarises the framework proposed in this paper for the Euler-Lagrange modelling of dilute particle-laden flows with arbitrary particle-size to mesh-spacing ratio, and conclusions are drawn in Section 6.

2. Governing equations

2.1. Equations of motion of the carrying fluid phase

The two-way coupled EL modelling of dilute particle-laden incompressible flow can be addressed using the following formulation of the Navier-Stokes equations [8]

$$\nabla \cdot \mathbf{u}_\mathrm{f} = 0\,, \tag{1a}$$

$$\rho_\mathrm{f}\left[\frac{\partial \mathbf{u}_\mathrm{f}}{\partial t} + \nabla\cdot(\mathbf{u}_\mathrm{f}\otimes\mathbf{u}_\mathrm{f})\right] = -\nabla p + \mu_\mathrm{f}\Delta\mathbf{u}_\mathrm{f} + \rho_\mathrm{f}\mathbf{g} + \mathbf{M}\,, \tag{1b}$$

where ρ_f is the fluid density, μ_f is the fluid dynamic viscosity, $\mathbf{u}_\mathrm{f} = u_\mathrm{f}\mathbf{e}_x + v_\mathrm{f}\mathbf{e}_y + w_\mathrm{f}\mathbf{e}_z$ is the fluid velocity vector, p is the pressure, and $\mathbf{g}$ is the gravity vector. $\mathbf{M}$ is the momentum transfer from the Lagrangian phase to the Eulerian phase, which reads as [14]

$$\mathbf{M} = -\sum_\mathrm{p} k(\|\mathbf{x}-\mathbf{x}_\mathrm{p}\|)\,\mathbf{f}_{\mathrm{p,fluid}}\,, \tag{2}$$

where $\sum_\mathrm{p}$ corresponds to the summation over all Lagrangian particles, $\mathbf{x}_\mathrm{p}$ is the centre of particle p, $\mathbf{f}_{\mathrm{p,fluid}}$ corresponds to the fluid forces acting on particle p (typically: drag), and k is a regularisation kernel, *i.e.* a smooth approximation of the

Dirac delta function, here chosen as a radial function associated with a length-scale ϵ, monotonically decreasing on $\mathbb{R}_+$, and normalised so that

$$\int_{\mathbb{R}^3} k(\|\mathbf{x}\|)\,\mathrm{d}\mathbf{x} = 1\,. \tag{3}$$

2.2. Equation of motion of a Lagrangian particle

The motion of a rigid spherical particle in a surrounding flow can be described by the Maxey-Riley-Gatignol equation [26, 27], which reads as

$$\rho_\mathrm{p} V_\mathrm{p} \frac{\mathrm{d}\mathbf{u}_\mathrm{p}}{\mathrm{d}t} = \rho_\mathrm{f} V_\mathrm{p} \frac{\mathcal{D}\tilde{\mathbf{u}}_{\mathrm{f@p}}}{\mathcal{D}t} + (\rho_\mathrm{p} - \rho_\mathrm{f}) V_\mathrm{p}\,\mathbf{g} + \mathbf{f}_{\mathrm{p,drag}} + \mathbf{f}_{\mathrm{p,add}} + \mathbf{f}_{\mathrm{p,history}}\,, \tag{4}$$

where V_p is the volume of the particle, $\mathbf{u}_\mathrm{p}$ is the particle velocity vector, $\tilde{\mathbf{u}}_{\mathrm{f@p}}$ is the "undisturbed" fluid velocity at the location of the particle, that is the local fluid velocity from which the disturbance due to the presence of particle p is subtracted, $\mathcal{D}(\cdot)/\mathcal{D}t$ is the time derivative following a fluid element, $\mathbf{f}_{\mathrm{p,add}}$ represents the added-mass force (which accounts for the acceleration of the fluid surrounding an accelerating particle), and $\mathbf{f}_{\mathrm{p,history}}$ is the Basset history force (arising from the time necessary to develop the boundary layers). For the purpose of this study, however, the following simplified form is used, neglecting all forces apart from gravity, buoyancy and drag,

$$\rho_\mathrm{p} V_\mathrm{p} \frac{\mathrm{d}\mathbf{u}_\mathrm{p}}{\mathrm{d}t} = (\rho_\mathrm{p} - \rho_\mathrm{f}) V_\mathrm{p}\,\mathbf{g} + \mathbf{f}_{\mathrm{p,drag}}\,. \tag{5}$$

Based on this simplified formulation, the fluid force acting on the particle is therefore

$$\mathbf{f}_{\mathrm{p,fluid}} = \mathbf{f}_{\mathrm{p,drag}} - \rho_\mathrm{f} V_\mathrm{p}\,\mathbf{g}\,. \tag{6}$$

The pressure gradient force, the added-mass force, and the Basset history force are neglected in this paper. Their consideration, however, would leave the analysis conducted in this paper unchanged, since the derivation conducted in Section 4.2 makes no assumption on the nature of the momentum transfer between the particles and the fluid.

The drag force is defined as

$$\mathbf{f}_{\mathrm{p,drag}} = \frac{3}{4}\frac{\rho_\mathrm{f} V_\mathrm{p} \mathrm{C_D}}{d_\mathrm{p}} \|\tilde{\mathbf{u}}_{\mathrm{f@p}} - \mathbf{u}_\mathrm{p}\| (\tilde{\mathbf{u}}_{\mathrm{f@p}} - \mathbf{u}_\mathrm{p})\,, \tag{7}$$

where d_p is the diameter of the particle, and the drag coefficient $\mathrm{C_D}$ is based on Stokes' drag law extended with the correlation of Schiller and Naumann [29], yielding

$$\mathrm{C_D} = \begin{cases} 24\left(1 + 0.15\,\mathrm{Re_p^{0.687}}\right)/\mathrm{Re_p} & \text{if } \mathrm{Re_p} \leq 800 \\ 0.44 & \text{otherwise} \end{cases}\,. \tag{8}$$

$\mathrm{Re_p}$ is the Reynolds number of the particle based on the local relative velocity, defined as

$$\mathrm{Re_p} = \frac{\rho_\mathrm{f} \|\tilde{\mathbf{u}}_{\mathrm{f@p}} - \mathbf{u}_\mathrm{p}\|\, d_\mathrm{p}}{\mu_\mathrm{f}}\,. \tag{9}$$

3. Source term regularisation

The choice of a *regularisation kernel function* (also referred to as *filter kernel function*) naturally influences the development and execution of the EL method, since it dictates the way momentum is transferred from the Lagrangian particles to the Eulerian fluid. The vast majority of approaches proposed in the literature to deal with arbitrarily sized particles rely on the Gaussian kernel to provide a smooth approximation of the Dirac delta function [14,18,20,23,24,30]. It is given as

$$g_\sigma(r) = \frac{1}{\left(2\pi\sigma^2\right)^{3/2}} \exp\left(\frac{-r^2}{2\sigma^2}\right), \qquad g_\sigma \in C^\infty(\mathbb{R})\,, \tag{10}$$

where r corresponds to the distance from the origin, and σ is the length-scale associated with the Gaussian: its standard deviation. On a Cartesian mesh, the discrete filter value in the cell $\mathrm{K} = [x_0, x_1] \times [y_0, y_1] \times [z_0, z_1]$ associated with a particle located at $\mathbf{x}_\mathrm{p}$ can directly be calculated using

$$g_{\sigma,\mathrm{K}}(\mathbf{x}_\mathrm{p}) = \frac{1}{V_\mathrm{K}} \int_\mathrm{K} g_\sigma(\|\mathbf{x} - \mathbf{x}_\mathrm{p}\|)\,\mathrm{d}\mathbf{x} = \frac{\left[\mathrm{erf}\left(\frac{x - x_\mathrm{p}}{\sigma\sqrt{2}}\right)\right]_{x_0}^{x_1}\left[\mathrm{erf}\left(\frac{y - y_\mathrm{p}}{\sigma\sqrt{2}}\right)\right]_{y_0}^{y_1}\left[\mathrm{erf}\left(\frac{z - z_\mathrm{p}}{\sigma\sqrt{2}}\right)\right]_{z_0}^{z_1}}{8\,(x_1 - x_0)(y_1 - y_0)(z_1 - z_0)}\,, \tag{11}$$

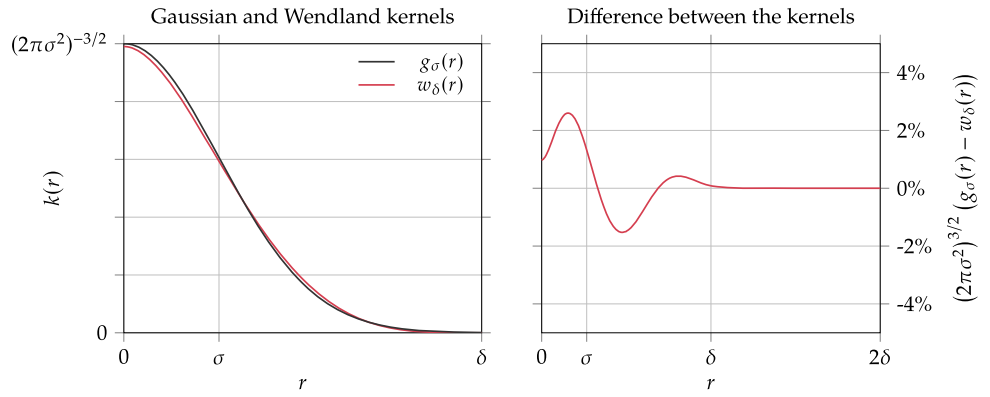

Fig. 1. Comparison between "equivalent" Gaussian and Wendland kernels (that is for $\sigma = \delta\sqrt{2/9\pi}$). Left: plot of both kernel functions as $r \in [0, \delta]$; Right: plot of the normalised difference between the Gaussian and Wendland kernels, whose maximum reaches about 2.6%.

where V_K is the volume of K. Alternatively (and more generally), the discrete filter values can be obtained from the solution of a diffusion equation [18,20], or using numerical integration [19]. In the present study, we propose to use a regularisation kernel based on the family of Wendland functions [31]. It is defined as

$$w_\delta(r) = \frac{21}{2\pi\delta^3}\begin{cases} (4r/\delta + 1)\,(1 - r/\delta)^4 & \text{if} \quad 0 \le r \le \delta \\ 0 & \text{if} \quad r > \delta \end{cases}, \qquad w_\delta \in C^2\left(\mathbb{R}_+\right), \tag{12}$$

and is smooth (enough, for the purpose of this paper), normalised, and compactly supported on the sphere of radius δ. When both the Wendland and Gaussian kernels have the same normalised integral over the real half-line, their respective length-scales are linked by the relation $\sigma = \delta\sqrt{2/9\pi}$ [31]. In this configuration, the Wendland kernel defined in Eq. (12) does not differ from the Gaussian kernel by more than 3%,[1] for any $r \in \mathbb{R}_+$, as illustrated in Fig. 1. The Wendland kernel does, however, present the advantage of having a simple polynomial form that allows – as shall be shown in Section 4 – to derive a concise polynomial expression of the averaged particle-induced flow disturbance. In the numerical tests conducted in this paper, the discrete value of the Wendland regularisation kernel in the computational cell K,

$$w_{\delta,\mathrm{K}}(\mathbf{x}_\mathrm{p}) = \frac{1}{V_\mathrm{K}}\int_\mathrm{K} w_\delta(\|\mathbf{x} - \mathbf{x}_\mathrm{p}\|)\,\mathrm{d}\mathbf{x}, \tag{13}$$

is estimated using the adaptive numerical integration procedure proposed in [19]. This approach selects an optimal number of numerical integration points as to estimate the integral of w_δ in the cell with arbitrary accuracy, regardless of the ratio δ/h (with $h = \sqrt[3]{V_\mathrm{K}}$) [19]. This means that we can control the error associated with the regularisation of the momentum source, and therefore eliminate this bias in the study of the accuracy of the velocity correction proposed in Section 4.

4. Recovery of the undisturbed flow velocity

The reduced model used to evaluate drag assumes knowledge of the undisturbed velocity at the location of the particle, that is the corresponding local fluid velocity as if the particle under consideration has no impact on the flow. In a two-way coupled EL context, the recovery of the undisturbed velocity at the location of a given particle is, generally, not a trivial task. Our choice of polynomial regularisation function, however, allows to derive a simple, exact, polynomial expression of the disturbance of the flow due to the particle momentum contribution, in the Stokes regime, which in turn can be integrated analytically. This results in a convergent and straightforward polynomial correction for the locally averaged flow disturbance. This derivation is conducted in the following sections, and subsequently extended to finite Reynolds numbers using Oseen's approximation.

4.1. Stokes flow through a regularised momentum source

Let us consider the very low Reynolds number, creeping flow steady-state regime, neglecting gravity. The governing equations (1a) and (1b) then reduce to

$$\nabla \cdot \mathbf{u}_\mathrm{f} = 0\,, \tag{14a}$$

$$-\nabla p + \mu_\mathrm{f}\,\Delta\mathbf{u}_\mathrm{f} + \mathbf{M} = 0\,. \tag{14b}$$

[1] In fact, it has been shown that the Wendland functions tend towards the Gaussian as their order is increased [31,32].

Placing oneself in the frame of reference of a single isolated particle moving at constant velocity, the equations become

$$\nabla \cdot \mathbf{u}_\mathrm{f} = 0\,, \tag{15a}$$

$$-\nabla p + \mu_\mathrm{f}\,\Delta \mathbf{u}_\mathrm{f} + \mathbf{f}_\mathrm{p}\,k(\|\mathbf{x}\|) = 0\,, \tag{15b}$$

with $\mathbf{f}_\mathrm{p}$ the opposite of the fluid force acting on the particle in a steady-state configuration, and k the regularisation kernel defined in Section 3. Note that $\mathbf{u}_\mathrm{f}$ is then the velocity of the flow relative to that of the particle. This corresponds to the case of a single, fixed, regularised momentum source located at the centre of an infinitely large domain, whose solution can be referred to as the *regularised Stokeslet* [33]. In the rest of this section, we derive an analytical expression for this regularised Stokeslet using the Wendland regularisation kernel. The first part of this derivation reproduces the general expression for the regularised Stokeslet presented by Cortez [33].

Applying the divergence operator to the momentum equation and based on the solenoidal nature of the field $\mathbf{u}_\mathrm{f}$, the momentum equation becomes

$$\Delta p = \mathbf{f}_\mathrm{p} \cdot \nabla k\,. \tag{16}$$

The solution to this equation is

$$p = \mathbf{f}_\mathrm{p} \cdot \nabla G_\epsilon\,, \tag{17}$$

with G_ϵ a *regularised* Green's function for the Laplacian, which is the solution to

$$\Delta G_\epsilon = k\,. \tag{18}$$

The regularised Green's function for the Laplacian G_ϵ presents the advantage of being smooth and bounded near zero (contrary to the *classical* Green's function for the Laplacian) [33]. Replacing pressure by this derived solution in the momentum equation, we obtain

$$\mu_\mathrm{f}\,\Delta \mathbf{u}_\mathrm{f} = (\mathbf{f}_\mathrm{p} \cdot \nabla)\nabla G_\epsilon - \mathbf{f}_\mathrm{p}\,k\,. \tag{19}$$

The solution to this equation reads as [33]

$$\mathbf{u}_\mathrm{f} = \frac{1}{\mu_\mathrm{f}}\left((\mathbf{f}_\mathrm{p} \cdot \nabla)\nabla B_\epsilon - \mathbf{f}_\mathrm{p} G_\epsilon\right) + \mathbf{K}\,, \tag{20}$$

where, following the same formalism as for G_ϵ, B_ϵ is the solution of the bi-harmonic equation

$$\Delta^2 B_\epsilon = k\,, \tag{21}$$

originating from the Poisson equation

$$\Delta B_\epsilon = G_\epsilon\,. \tag{22}$$

The solution provided in Eq. (20) can be referred to as the *regularised Stokeslet* velocity [33]. This regularised Stokeslet velocity is defined within a constant vector $\mathbf{K}$ that can be determined from the value of the far-field velocity. Since k, the kernel with which the particle momentum source is regularised, is a radial function, the regularised Green's functions for the Laplacian and bi-harmonic operators, G_ϵ and B_ϵ, are also radial. We can therefore write that

$$\nabla G_\epsilon = G'_\epsilon(r)\frac{\mathbf{x}}{r}\,, \tag{23}$$

(and similarly for B_ϵ). The first term of the right-hand side of Eq. (20) thus becomes

$$(\mathbf{f}_\mathrm{p} \cdot \nabla)\nabla B_\epsilon = (\mathbf{f}_\mathrm{p} \cdot \nabla)\left(B'_\epsilon(r)\frac{\mathbf{x}}{r}\right) = \mathbf{f}_\mathrm{p}\frac{B'_\epsilon(r)}{r} + (\mathbf{f}_\mathrm{p} \cdot \mathbf{x})\,\mathbf{x}\left(\frac{rB''_\epsilon(r) - B'_\epsilon(r)}{r^3}\right)\,, \tag{24}$$

and the regularised Stokeslet velocity reads as [33]

$$\mathbf{u}_\mathrm{f} = \frac{1}{\mu_\mathrm{f}}\left(\mathbf{f}_\mathrm{p}\left(\frac{B'_\epsilon(r)}{r} - G_\epsilon(r)\right) + (\mathbf{f}_\mathrm{p} \cdot \mathbf{x})\,\mathbf{x}\left(\frac{rB''_\epsilon(r) - B'_\epsilon(r)}{r^3}\right)\right) + \mathbf{K}\,. \tag{25}$$

We now apply the Wendland kernel defined in Eq. (12) as the regularisation kernel k, and assume, without loss of generality, that $\mathbf{f}_\mathrm{p} = f_\mathrm{p}\,\mathbf{e}_x$. The regularised Stokeslet velocity along the x-direction, *i.e.* along the direction of the forcing $\mathbf{f}_\mathrm{p}$, is then given by

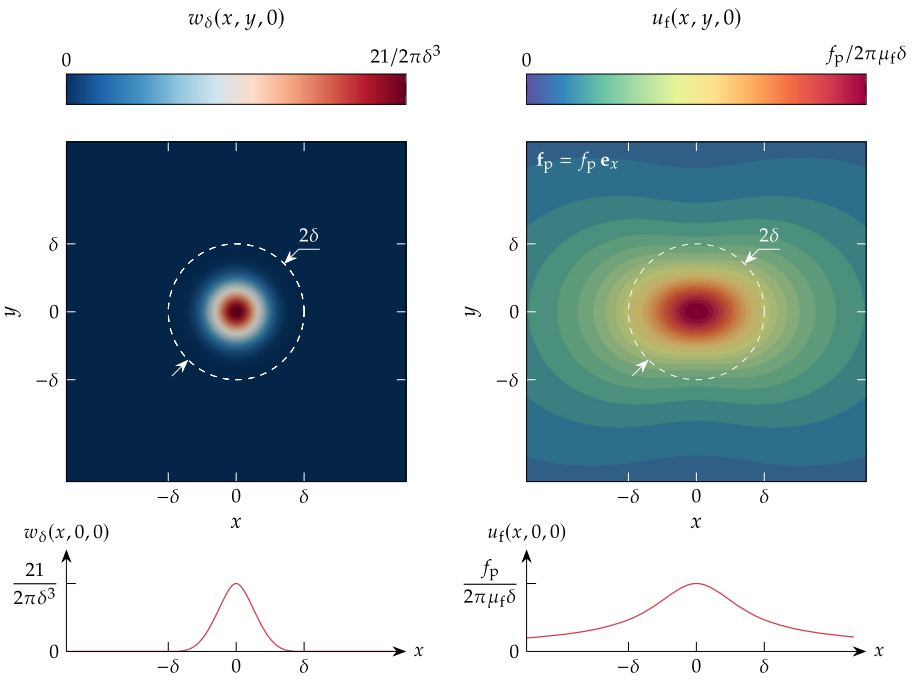

Fig. 2. Illustration of the kernel function field and x-velocity field resulting from the presence of a single fixed particle at the origin of the domain, in the Stokes regime, with $\delta = 4r_\mathrm{p}$ and a momentum transfer term $\mathbf{M} = \mathbf{f}_\mathrm{p}\, w_\delta(\|\mathbf{x}\|) = f_\mathrm{p}\, w_\delta(\|\mathbf{x}\|)\,\mathbf{e}_x$. The top left and right plots show the kernel function and x-velocity fields in the $z=0$ plane; the bottom left and right plots show the filter function and x-velocity fields on the $(y=0, z=0)$ line.

$$u_\mathrm{f}(\hat{r},\theta,\phi) = \frac{f_\mathrm{p}}{120\,\mu_\mathrm{f}\,\delta\,\pi\,\hat{r}^3}\begin{cases} (63\hat{r}^{10} - 300\hat{r}^9 + 525\hat{r}^8 - 360\hat{r}^7 + 84\hat{r}^5)(\sin\theta)^2(\cos\phi)^2 \\ \quad - 81\hat{r}^{10} + 400\hat{r}^9 - 735\hat{r}^8 + 540\hat{r}^7 - 168\hat{r}^5 + 60\hat{r}^3 & \text{if } 0 \le \hat{r} \le 1 \\ (15\hat{r}^2 - 3)(\sin\theta)^2(\cos\phi)^2 + 15\hat{r}^2 + 1 & \text{if } \hat{r} > 1 \end{cases}, \tag{26}$$

where $(\hat{r},\theta,\phi)$ are the normalised spherical coordinate variables, which relate to the Cartesian coordinate variables (x,y,z) following

$$\begin{cases} x &= \delta\,\hat{r}\,\sin\theta\,\cos\phi \\ y &= \delta\,\hat{r}\,\sin\theta\,\sin\phi \\ z &= \delta\,\hat{r}\,\cos\theta \end{cases}. \tag{27}$$

The component $\hat{r}$ is the normalised radius,

$$\hat{r} = \frac{r}{\delta} = \frac{\sqrt{x^2+y^2+z^2}}{\delta}, \tag{28}$$

where δ is the length-scale of the Wendland kernel (defined as the radius of its compact support). The detailed derivation leading to Eq. (26) can be found in Appendix A. This regularised Stokeslet velocity field is illustrated in Fig. 2, alongside the corresponding Wendland kernel function used to regularise the momentum contribution of the particle.

4.2. Recovery of the undisturbed flow velocity

4.2.1. Point-wise velocity correction

Based on the expression for the regularised Stokeslet velocity, Eq. (25), the intensity of the velocity disturbance induced by the regularised momentum source at the origin, *i.e.* at the centre of the particle, is given by

$$u_\mathrm{f}(\mathbf{0}) = \|\mathbf{K}\| = \frac{f_\mathrm{p}}{2\,\pi\,\mu_\mathrm{f}\,\delta}. \tag{29}$$

Remarkably, with $\sigma = \delta\sqrt{2/9\pi}$, that is when the Gaussian and Wendland kernels have the same normalised integral over the real half-line, this reads as

$$u_\mathrm{f}(\mathbf{0}) = \frac{f_\mathrm{p}}{3\,\pi\sqrt{2\pi}\,\mu_\mathrm{f}\,\sigma}, \tag{30}$$

which is the formula obtained by Balachandar et al. [14] using a Gaussian kernel to regularise the momentum transfer term. The use of the Gaussian or the Wendland kernel results in the same velocity disturbance at the centre of the particle, provided that $\sigma = \delta\sqrt{2/9\pi}$ (even though the flow differs elsewhere in the domain). Returning to the frame of reference of the fixed flow domain and for a particle moving in an arbitrary direction, the undisturbed flow velocity at the centre of the particle can thus be recovered using

$$\tilde{\mathbf{u}}_{\mathrm{f@p}} = \mathbf{u}_{\mathrm{f@p}} - \frac{\mathbf{f}_\mathrm{p}}{2\,\pi\,\mu_\mathrm{f}\,\delta}\,, \tag{31}$$

where $\mathbf{u}_{\mathrm{f@p}}$ is the flow velocity interpolated to the centre of the particle p, and $\tilde{\mathbf{u}}_{\mathrm{f@p}}$ the corresponding point-wise "undisturbed" velocity, that is the flow velocity at the centre of the particle p from which the flow disturbance due to the presence of the particle is subtracted.

4.2.2. Averaged velocity correction

The interpolation of the undisturbed flow velocity to the centre of the particle for the estimation of drag may, in some cases, be inaccurate. For particles that are larger than the computational cells, this quantity involves scales of the fluid motion that are smaller than the particle. Stokes' drag law (and its extension to finite Reynolds number regimes) is derived from the integration of the stresses acting on the particle boundary in uniform flow. Averaging the flow velocity over a volume that somehow scales with the particle, as opposed to using the velocity interpolated to the centre of the particle, is thus consistent with the underlying hypothesis of Stokes' law. To illustrate this, consider a velocity field available on the Eulerian mesh that is split in the form $\mathbf{u}_\mathrm{f} = \bar{\mathbf{u}}_\mathrm{f} + \mathbf{u}'_\mathrm{f}$, where $\bar{\mathbf{u}}_\mathrm{f}$ corresponds to the scales of the flow that are larger than the particle, and $\mathbf{u}'_\mathrm{f}$ to the scales that are smaller than the particle. As such, $\bar{\mathbf{u}}_\mathrm{f}$ varies little across the particle. The value of $\bar{\mathbf{u}}_\mathrm{f}$ at the centre of the particle thus accurately approximates its value on the particle boundary, and is therefore representative of the magnitude of the integral of the viscous stresses acting on the particle boundary. The component $\mathbf{u}'_\mathrm{f}$, on the other hand, can vary substantially across the particle, so its value at the centre of the particle does not necessarily correspond to its value at the particle boundary. The value of $\mathbf{u}'_\mathrm{f}$ interpolated to the centre of the particle thus provides little to no information regarding the impact of the small scales of the flow on the magnitude of the drag force acting on the particle. Based on these premises, we propose to consider a locally averaged velocity for the estimation of drag [23,24]. This averaged velocity is obtained by convoluting the available velocity field with the Wendland kernel defined in Eq. (12). We define the velocity averaging operator as

$$\mathcal{A}(\mathbf{u}_\mathrm{f})_{\mathrm{@p}} = \int_{\mathbb{R}^3} \mathbf{u}_\mathrm{f}(\mathbf{x})\, w_\lambda(\|\mathbf{x} - \mathbf{x}_\mathrm{p}\|)\,\mathrm{d}\mathbf{x}\,, \tag{32}$$

where w_λ is the normalised Wendland kernel with support radius λ, and $\mathbf{x}_\mathrm{p}$ the centre of particle p. The support radius λ should be of the order of the particle diameter, so that the scales of the fluid motion that are filtered out by the averaging operator are those that are smaller than the particle. The intensity of the velocity disturbance averaged at the centre of the particle, using the proposed averaging operator, is then given by

$$\mathcal{A}(u_\mathrm{f})_{\mathrm{@p}} = \int_0^{2\pi}\int_0^{\pi}\int_0^{\infty} w_\lambda(r)\, u_\mathrm{f}(r,\theta,\phi)\, r^2\, \sin\theta\,\mathrm{d}r\,\mathrm{d}\theta\,\mathrm{d}\phi\,, \tag{33}$$

which, with the variable change $\hat{r} = r/\delta$ and due to the compact nature of w_λ, also reads as

$$\mathcal{A}(u_\mathrm{f})_{\mathrm{@p}} = \int_0^{2\pi}\int_0^{\pi}\int_0^{\lambda/\delta} \frac{21\,\delta^3}{2\pi\,\lambda^3}(4\,\hat{r}\,\delta/\lambda + 1)(1 - \hat{r}\,\delta/\lambda)^4\, u_\mathrm{f}(\hat{r},\theta,\phi)\,\hat{r}^2\, \sin\theta\,\mathrm{d}\hat{r}\,\mathrm{d}\theta\,\mathrm{d}\phi\,. \tag{34}$$

Using the expression for the regularised Stokeslet velocity given in Eq. (26), the previous equation can be shown to reduce to

$$\mathcal{A}(u_\mathrm{f})_{\mathrm{@p}} = \frac{\Psi_{\mathrm{Stk}}(\lambda/\delta)\, f_\mathrm{p}}{2\,\pi\,\mu_\mathrm{f}\,\delta}\,, \tag{35}$$

with

$$\Psi_{\mathrm{Stk}}(x) = \frac{1}{2145}\begin{cases} 2145 - 1001\,x^2 + 910\,x^4 - 735\,x^5 + 250\,x^6 - 33\,x^7 & \text{if } 0 \le x \le 1 \\ 2145/x - 1001/x^3 + 910/x^5 - 735/x^6 + 250/x^7 - 33/x^8 & \text{if } x > 1 \end{cases}. \tag{36}$$

The function Ψ_{Stk} is illustrated in Fig. 3. Note that, should we have chosen the Gaussian kernel as source term regularisation kernel at the beginning of this paper, determining Ψ_{Stk} would then require numerical integration, thereby losing the generality of the expression in Eq. (36).

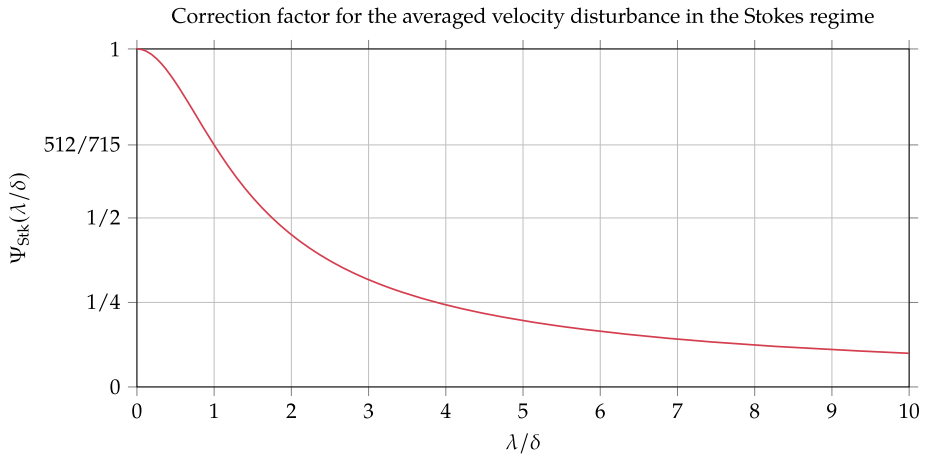

Fig. 3. Correction factor for the averaged velocity disturbance in the Stokes regime. Note that for the case $\lambda = 0$, the function is equal to 1 meaning that the point-value of velocity given in Eq. (29) is recovered.

Returning to the fixed frame of reference of the flow domain and for a particle moving in an arbitrary direction, the averaged undisturbed velocity for particle p can be recovered using

$$\mathcal{A}(\tilde{\mathbf{u}}_{\mathrm{f}})_{@\mathrm{p}} = \mathcal{A}(\mathbf{u}_{\mathrm{f}})_{@\mathrm{p}} - \frac{\Psi_{\mathrm{Stk}}(\lambda/\delta)\,\mathbf{f}_{\mathrm{p}}}{2\pi\,\mu_{\mathrm{f}}\,\delta}\,, \tag{37}$$

where $\mathcal{A}(\mathbf{u}_{\mathrm{f}})_{@\mathrm{p}}$ is the flow velocity averaged at the centre of the particle p using the averaging operator defined in Eq. (32), and $\mathcal{A}(\tilde{\mathbf{u}}_{\mathrm{f}})_{@\mathrm{p}}$ the corresponding averaged "undisturbed" velocity, that is the flow velocity averaged at the centre of the particle p from which the flow disturbance due to the presence of the particle is subtracted. Note that as $\lambda/\delta \to 0$, Eq. (31) is recovered from Eq. (37) since $\Psi_{\mathrm{Stk}}(0) = 1$, $\lim_{\lambda\to 0}\mathcal{A}(\mathbf{u}_{\mathrm{f}})_{@\mathrm{p}} = \mathbf{u}_{\mathrm{f}@\mathrm{p}}$, and $\lim_{\lambda\to 0}\mathcal{A}(\tilde{\mathbf{u}}_{\mathrm{f}})_{@\mathrm{p}} = \tilde{\mathbf{u}}_{\mathrm{f}@\mathrm{p}}$.

In addition to being consistent with the underlying hypothesis of Stokes' law, note that considering the locally averaged undisturbed velocity for the estimation of drag, combined with the choice of length-scales $\delta = \lambda = 1536\,r_{\mathrm{p}}/715$ (with r_{p} the particle radius), allows for a consistent energy balance between the particle and the fluid, in the Stokes regime [23]. This point is demonstrated in Appendix B.

4.3. The regularisation scale

The choice of a value for the radius of the regularisation support, δ, can naturally have a large impact on the results of two-way coupled EL simulations, even more so when the particles are large compared to the mesh cells. If δ tends to 0, then the regularisation kernel will tend towards the Dirac delta function, resulting in a locally singular velocity. To the contrary, a very large value of δ means that the momentum contribution of the particle will locally be very small and have no significant impact on the flow. There is a prevailing consensus within the community that δ should relate to the particle radius, and have a typical value of "a few radii" [14,18,20,23,24,30]. This yields a momentum contribution that is confined to the vicinity of the particle while resulting in a moderate local velocity disturbance.

Since the flow through the regularised momentum contribution of a particle is known (cf. Section 4.1), it is actually possible to choose values of δ that allow to match the velocity of the local flow with that of the Lagrangian particle (at least in the Stokes regime). We propose three such options:

Centre velocity match One may, for instance, want the point-wise flow velocity at the centre of the particle to be equal to that of the particle. Assuming that Stokes' drag law applies and is based on this point-wise velocity, then the opposite of the drag force acting on the particle is given by

$$\mathbf{f}_{\mathrm{p}} = 6\pi\,\mu_{\mathrm{f}}\,r_{\mathrm{p}}\,(\mathbf{u}_{\mathrm{p}} - \tilde{\mathbf{u}}_{\mathrm{f}@\mathrm{p}})\,, \tag{38}$$

which, inserted into Eq. (31), yields

$$\tilde{\mathbf{u}}_{\mathrm{f}@\mathrm{p}} = \mathbf{u}_{\mathrm{f}@\mathrm{p}} - \frac{6\pi\,\mu_{\mathrm{f}}\,r_{\mathrm{p}}\,(\mathbf{u}_{\mathrm{p}} - \tilde{\mathbf{u}}_{\mathrm{f}@\mathrm{p}})}{2\pi\,\mu_{\mathrm{f}}\,\delta}\,. \tag{39}$$

If $\mathbf{u}_{\mathrm{p}} = \mathbf{u}_{\mathrm{f}@\mathrm{p}}$, this results in

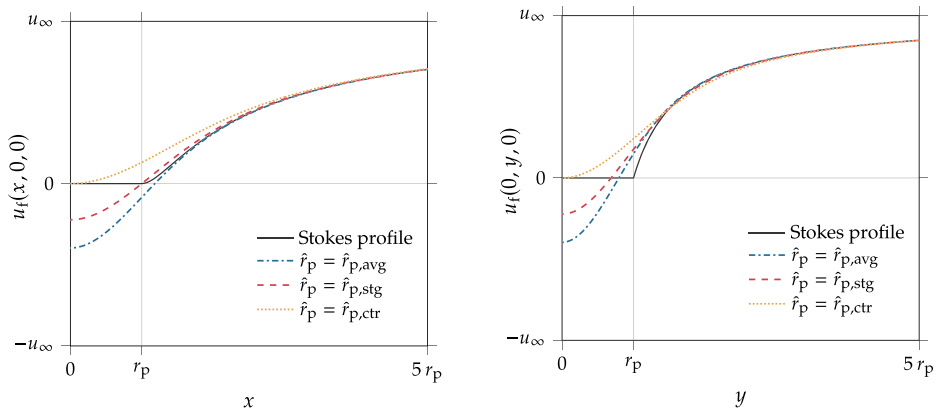

Fig. 4. Profiles of the x-component of velocity over the lines $(y=0, z=0)$ and $(x=0, z=0)$, for the Stokes flow through a regularised momentum source, for varying values of $\hat{r}_p = r_p/\delta$.

$$\frac{r_p}{\delta} = \hat{r}_{p,ctr} = \frac{1}{3}\,. \tag{40}$$

This value corresponds to the ratio $r_p/\sigma = \sqrt{\pi/2}$ derived by Maxey and Patel [23] for the Gaussian kernel.

Averaged velocity match Similarly, one may want the averaged velocity at the centre of the particle to be equal to that of the particle (we consider the case $\lambda = \delta$). Assuming that drag is based on this averaged velocity, then the opposite of the drag force acting on the particle is given by

$$\mathbf{f}_p = 6\pi\,\mu_f r_p\,(\mathbf{u}_p - \mathcal{A}(\tilde{\mathbf{u}}_f)_{@p})\,, \tag{41}$$

which, inserted into Eq. (37), yields

$$\mathcal{A}(\tilde{\mathbf{u}}_f)_{@p} = \mathcal{A}(\mathbf{u}_f)_{@p} - \frac{\Psi_{Stk}(1)\,6\pi\,\mu_f r_p\,(\mathbf{u}_p - \mathcal{A}(\tilde{\mathbf{u}}_f)_{@p})}{2\pi\,\mu_f\delta}\,. \tag{42}$$

If $\mathbf{u}_p = \mathcal{A}(\mathbf{u}_f)_{@p}$, this results in

$$\frac{r_p}{\delta} = \hat{r}_{p,avg} = \frac{715}{1536}\,. \tag{43}$$

This value corresponds to the ratio $r_p/\sigma = \sqrt{\pi}$ derived by Maxey and Patel [23] for the Gaussian kernel. This approach allows for a consistent energy balance between the particle and the fluid [23], as is shown in Appendix B of this paper.

Stagnation point velocity match Finally, to get as close as possible to the actual Stokes flow around the sphere, one may want to enforce the flow velocity at the (fictitious) stagnation point in front of the particle to be equal to that of the particle. Using Eq. (26), considering a particle moving along the x-direction, this yields

$$u_f(r_p,0,0) - \tilde{u}_{f@p} = \frac{6\pi\,\mu_f r_p\,(u_p - \tilde{u}_{f@p})}{120\pi\,\mu_f\delta}\left(-18\,\hat{r}_p^7 + 100\,\hat{r}_p^6 - 210\,\hat{r}_p^5 + 180\,\hat{r}_p^4 - 84\,\hat{r}_p^2 + 60\right)\,, \tag{44}$$

whose solution, if $u_p = u_f(r_p,0,0)$, is

$$\frac{r_p}{\delta} = \hat{r}_{p,stg} \simeq 0.4075\,. \tag{45}$$

The velocity profiles along the axial and radial directions for the flow through a fixed momentum source, for the values of $\hat{r}_p$ corresponding to the three cases discussed above, are given in Fig. 4, while the streamlines of the velocity field for these flows are illustrated in Fig. 5. From Fig. 5, we observe that the streamlines of the flow for the case $\hat{r}_p = \hat{r}_{p,stg}$ are in excellent qualitative agreement with the streamlines of the analytical Stokes flow around the particle, although the no-slip condition is not explicitly enforced at the particle boundary.

4.4. Convergence study

The accuracy at finite mesh-resolution of the derived corrections is assessed through a convergence study, using our in-house finite-volume CFD research code `MultiFlow` (second-order accurate in time and space) [34]. The numerical test-case, illustrated in Fig. 6, considers the uniform flow over a fixed Lagrangian particle with $\mathrm{Re}_p = 0.01$. Correspondingly,

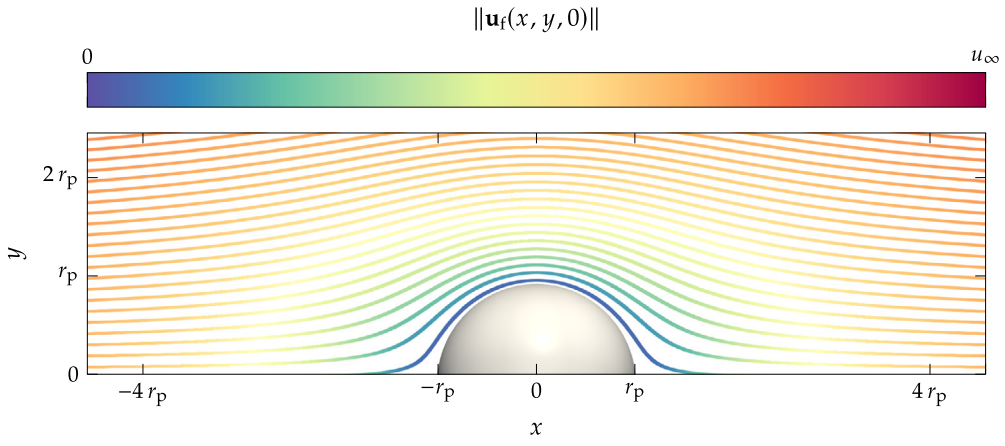

(a) Stokes flow around a sphere

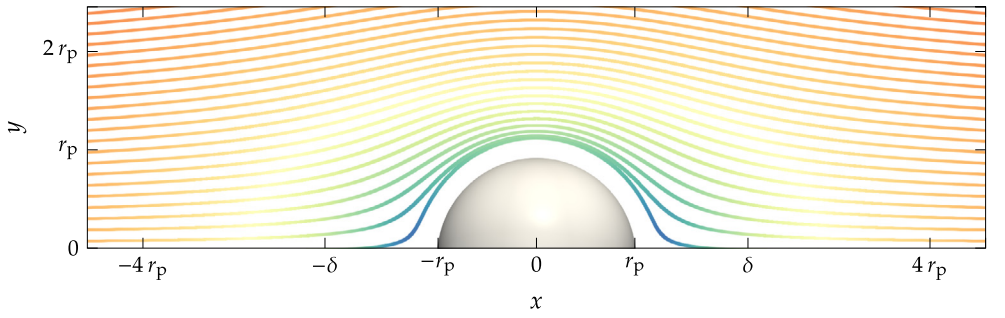

(b) Stokes flow through a regularised Stokes drag momentum source with $\delta = r_\mathrm{p}/\hat{r}_\mathrm{p,avg} = 1536\,r_\mathrm{p}/715$

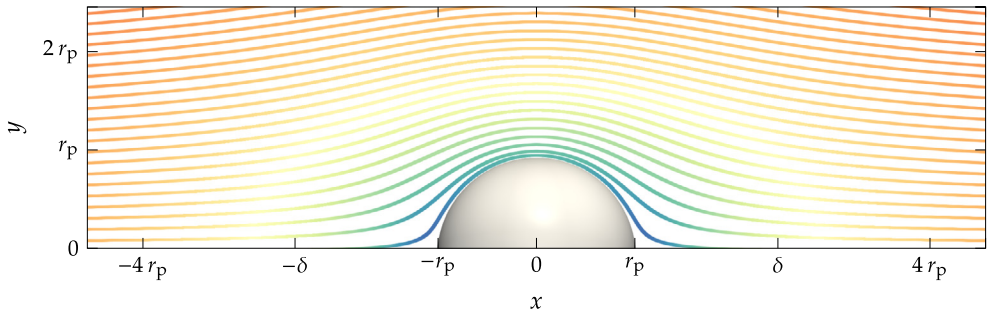

(c) Stokes flow through a regularised Stokes drag momentum source with $\delta = r_\mathrm{p}/\hat{r}_\mathrm{p,stg} \simeq 2.454\,r_\mathrm{p}$

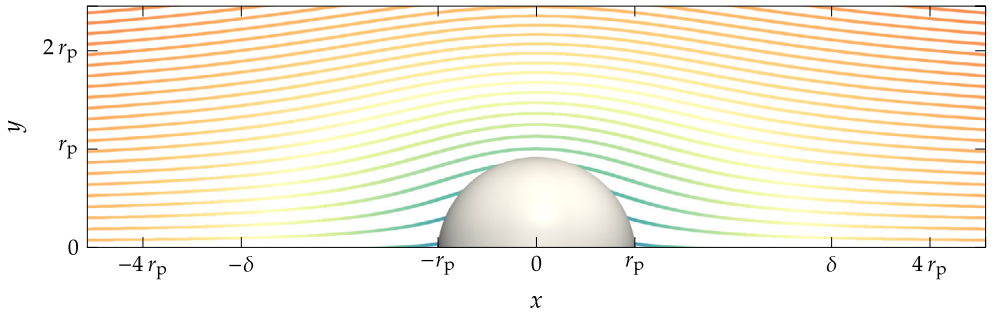

(d) Stokes flow through a regularised Stokes drag momentum source with $\delta = r_\mathrm{p}/\hat{r}_\mathrm{p,ctr} = 3\,r_\mathrm{p}$

Fig. 5. Streamlines of the velocity field for: (a) The Stokes flow around a sphere; (b) The Stokes flow through the corresponding regularised drag momentum source with $\hat{r}_\mathrm{p} = \hat{r}_\mathrm{p,avg}$; (c) The Stokes flow through the corresponding regularised drag momentum source with $\hat{r}_\mathrm{p} = \hat{r}_\mathrm{p,stg}$; (d) The Stokes flow through the corresponding regularised drag momentum source with $\hat{r}_\mathrm{p} = \hat{r}_\mathrm{p,ctr}$.

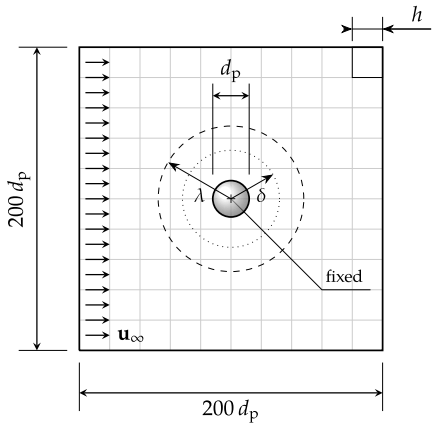

Fig. 6. Setup (illustration not to scale) for the convergence study on the uniform flow through a fixed Lagrangian particle, with $\mathrm{Re}_p = 0.01$.

a uniform velocity $\mathbf{u}_\infty$ is applied at the inlet boundary. In this configuration, the point-wise and averaged undisturbed velocities for the particle are equal to the far-field velocity, *i.e.* $\tilde{\mathbf{u}}_{f@p} = \mathcal{A}(\tilde{\mathbf{u}}_f)_{@p} = \mathbf{u}_\infty$. The momentum exchange from the Lagrangian particle to the Eulerian fluid is accounted for through a constant momentum source field,

$$\mathbf{M} = \mathbf{f}_p w_\delta(\|\mathbf{x}\|)\,, \tag{46}$$

where $\mathbf{f}_p$ is the opposite of the drag force acting on the isolated, fixed particle located in the centre of the domain, and w_δ is the regularisation kernel introduced in Section 3. The flow velocity field is initialised based on the exact solution derived in Section 4.1, and the flow solver is run until the solution has fully converged and a steady-state equilibrium has been reached. The radius of the support of the regularisation kernel is chosen as

$$\delta = \max(r_p/\hat{r}_p, h/2)\,, \tag{47}$$

where $\hat{r}_p$, the maximum ratio between the particle radius and the regularisation support radius, is varied between $1/4$ and 1, and h is the mesh spacing. A value of the radius δ that would be smaller than $h/2$ is non-sensical from the point of view of the numerics: the inevitable averaging due to the very nature of the finite-volume approach means that the minimum size of any regularisation support is the size of the mesh cell itself. To ensure an adequate resolution and smoothness of the averaging operation for velocity, the radius of the velocity averaging kernel support, λ, is chosen as

$$\lambda = \max(\delta, 2h) = \max(r_p/\hat{r}_p, 2h)\,. \tag{48}$$

Finally, the local mesh-spacing h is varied to yield particle-size to mesh-spacing ratios between $d_p/h = 0.01$ and $d_p/h = 10$, and the flow domain has a minimum size of $(200\,d_p)^3$ in order to avoid any discernible influence of the domain boundaries on the flow. A constant mesh spacing h is used in the vicinity of the particle, and is then stretched far away from the particle with a growth factor $f \lesssim 1.1$. The resulting mesh consists of, at most, 200^3 cells. The relative errors for the recovery of the (averaged) undisturbed flow velocity at the location of the particle are plotted in Figs. 7a and 7b.

In Fig. 7a, $\hat{r}_p$ is fixed to the value $1/4$ meaning that δ is no less than $4\,r_p$, and various approximations for the undisturbed velocity are compared. The following colour code is used:

1) (blue) corresponds to the error obtained if the point-wise velocity interpolated to the centre of the particle is used to approximate the undisturbed velocity,
2) (yellow) corresponds to the error obtained if the averaged velocity is used to approximate the undisturbed velocity,
3) (green) corresponds to the error obtained if the interpolated point-wise velocity corrected with Eq. (31) is used to approximate the undisturbed velocity,
4) (red) corresponds to the error obtained if the averaged velocity corrected with Eq. (37) is used to approximate the undisturbed velocity.

The first two error-lines (blue and yellow) illustrate the limitations of the classical PSIC-EL and filtered EL approaches. Indeed, using the uncorrected point-wise or averaged flow velocity as an approximation for the undisturbed flow velocity, we observe first-order convergence as d_p/h decreases below unity, owing to the associated linear decrease of the magnitude of the resolved flow disturbance, as is typically observed in the literature [16]. As d_p/h increases above unity, however, the errors stagnate. This is due to the regularisation length-scale being fixed and chosen proportional to the particle diameter – the flow disturbance induced by the transfer of momentum thus becomes independent of the mesh spacing as $d_p \gg h$. For

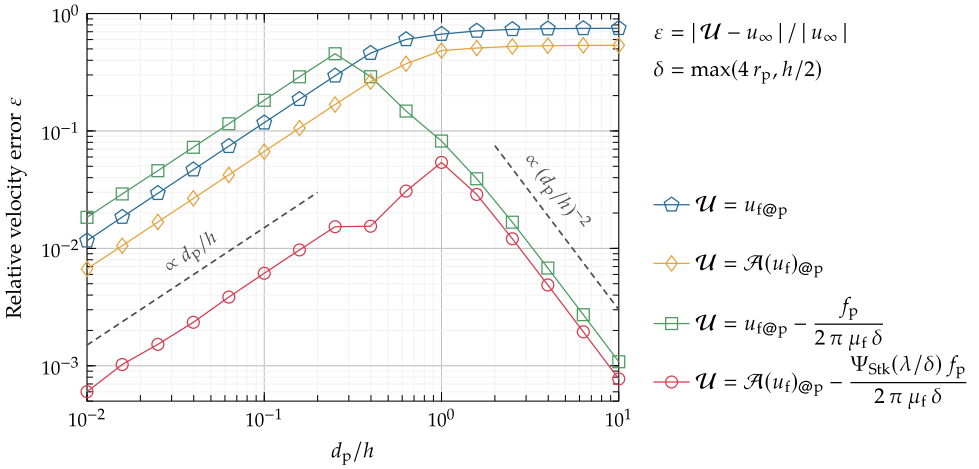

(a) For different approximations of the undisturbed flow velocity

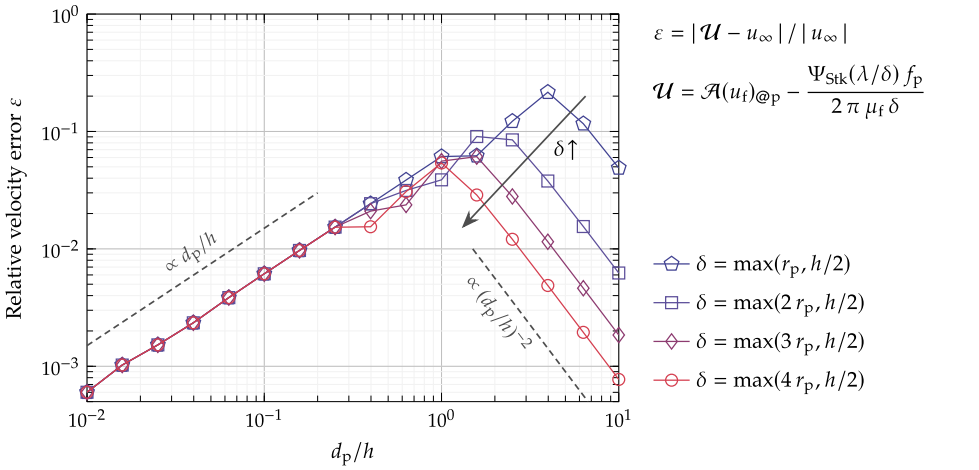

(b) For varying values of the regularisation support radius

Fig. 7. Study of the errors in reconstructing the point-wise or averaged undisturbed velocity at the location of a fixed, isolated particle at $\mathrm{Re}_p = 0.01$, when (a) varying the type of approximation for the undisturbed velocity; and (b) varying the maximum ratio between the particle radius and the regularisation support radius. The particle-size/mesh-spacing ratio is varied between $d_p/h = 0.01$ and $d_p/h = 10$.

large particles, for this case with $\hat{r}_p = 1/4$, the relative errors in the recovery of the (averaged) undisturbed velocity without applying any correction are of the order of 50% to 100%.

When applying the corrections derived in Eqs. (31) and (37), however, we observe a similar first-order convergence of the errors as d_p/h decreases below unity but also second-order convergence of the errors as d_p/h increases above unity – the largest error is found when $d_p \simeq h$. This second-order convergence behaviour simply corresponds to the order of accuracy of the flow solver, *i.e.* the order of accuracy with which `MultiFlow` is able to resolve the flow disturbance due to the regularised momentum source term. The peak of the errors when $d_p \simeq h$ is explained by a momentum transfer – and therefore a local flow disturbance – that is significant, combined with a relatively coarse mesh resolution of the kernel support ($\delta \simeq 2\,h$), resulting in a flow disturbance as resolved by the flow solver that is not well approximated by the analytical expression derived in Eq. (25).

It is also interesting to note that, although all approximations of the undisturbed velocity result in first-order convergence of the errors when d_p/h decreases below unity, the derived corrections have different impacts on the absolute values of these errors. The correction for the point-wise velocity interpolated to the centre of the particle results in larger values of the relative error than when no correction is used (as shown by the vertical shift between the blue and green lines). This is due to the mesh spacing being equal to the kernel support diameter for $d_p/h < 1$, meaning that the flow disturbance as computed on the mesh only poorly approximates the analytical field expressed in Eq. (25). The correction for the point-wise interpolated velocity, because it is based on the analytical field, thus overcorrects and therefore introduces an error that is larger than in the uncorrected case. Contrarily, the correction for the averaged velocity yields relative errors that are about an order of magnitude smaller than those obtained without correction (as shown by the vertical shift between the

yellow and red lines). This is due to the averaging support radius being at least equal to twice the mesh spacing, meaning that the averaged velocity disturbance as computed on the mesh is well approximated by the analytical solution given in Eq. (35). The correction for the averaged velocity presented in Eq. (37) can thus also improve the accuracy of classical PSIC-EL methods, at a very limited cost.

In Fig. 7b, $\hat{r}_\mathrm{p}$ is varied between 1/4 and 1, and the relative errors in estimating the averaged undisturbed velocity using Eq. (37) are compared. The lines are coloured based on the value of $\hat{r}_\mathrm{p}$. The same convergence behaviour as in Fig. 7a is logically observed. All lines collapse on one another as d_p/h decreases below unity, since δ is then equal to $h/2$ regardless of the value of $\hat{r}_\mathrm{p}$. As d_p/h increases above unity, a vertical shift is observed between the lines for different values of $\hat{r}_\mathrm{p}$, relating to the correspondingly different mesh-resolutions of the regularisation kernel (the larger $\hat{r}_\mathrm{p}$, *i.e.* the smaller δ/r_p, the larger the errors). Indeed, as explained previously in this section, the peak of the errors directly relates to a value of the ratio δ/h that is small, combined with a significant amount of momentum that is transferred from the particle to the fluid. Increasing $\hat{r}_\mathrm{p}$ (*i.e.* reducing δ/h for a given particle diameter) will then shift this peak towards higher values of d_p/h.

4.5. Finite Reynolds number correction

The previously derived averaged velocity correction is only valid for very small Reynolds numbers, *i.e.* creeping flow. Its extension to finite Reynolds numbers, through a similar analytical derivation, is not possible owing to the non-linearity of the governing flow equations. An alternative to such an analytical derivation would be to consider a set of numerical simulations with varying values of δ/r_p, λ/δ and Re_p, and to fit the coefficients of the polynomial $\Psi_\mathrm{Stk}(x)$ to their results. Such work has been conducted for a point-wise velocity correction [13,14]. Balachandar et al. [14], however, showed that the linearisation of the flow equations using Oseen's approximation allows to derive an analytical correction factor that agrees very well with the results of their numerical tests, for values of Re_σ, the Reynolds number associated with the Gaussian standard deviation σ, as large as 10^4. We thus conduct such a derivation for the framework presented in this paper.

Oseen's approximation consists in linearising the advection term of the momentum flow equations about the far-field velocity $\mathbf{u}_\infty$. The governing equations in the frame of reference of the particle, in a steady-state configuration, become

$$\nabla \cdot \mathbf{u}_\mathrm{f} = 0\,, \tag{49a}$$

$$-\nabla p + \mu_\mathrm{f}\,\Delta \mathbf{u}_\mathrm{f} + \mathbf{f}_\mathrm{p}\,k(\|\mathbf{x}\|) = \rho\,\mathbf{u}_\infty \cdot \nabla \mathbf{u}_\mathrm{f}\,. \tag{49b}$$

Considering $\mathbf{u}_\infty = u_\infty\,\mathbf{e}_x$ and $\mathbf{f}_\mathrm{p} = f_\mathrm{p}\,\mathbf{e}_x$, a configuration corresponding to $\mathbf{f}_\mathrm{p}$ being the opposite of the drag force acting on the particle due to the relative velocity $\mathbf{u}_\infty$, and normalising the equations with the regularisation scale ϵ and far-field velocity u_∞, the equations simplify to

$$\nabla \cdot \mathbf{u}_\mathrm{f}^\star = 0\,, \tag{50a}$$

$$-\nabla p^\star + \frac{1}{\mathrm{Re}_\epsilon}\Delta \mathbf{u}_\mathrm{f}^\star + f_\mathrm{p}^\star\,k^\star(\|\mathbf{x}\|)\mathbf{e}_x = \frac{\partial \mathbf{u}_\mathrm{f}^\star}{\partial x}\,, \tag{50b}$$

the superscript $\star$ indicating that the variables/functions are normalised with respect to the regularisation scale and far-field velocity. The normalised variables relate to the original variables following $\mathbf{u}_\mathrm{f}^\star = \mathbf{u}_\mathrm{f}/u_\infty$, $p^\star = p/\rho_\mathrm{f}\,u_\infty^2$, and $f_\mathrm{p}^\star = f_\mathrm{p}/\rho_\mathrm{f}\,u_\infty^2\,\epsilon^2$. The normalised Wendland and Gaussian kernels are such that $w_\delta^\star = w_{\delta/\epsilon}$ and $g_\sigma^\star = g_{\sigma/\epsilon}$. The three-dimensional Fourier transform of the normalised momentum equation yields [14]

$$\mathcal{F}(u_\mathrm{f}^\star)(\boldsymbol{\omega}) = \frac{\mathrm{Re}_\epsilon\left(1 - i\dfrac{\mathrm{Re}_\epsilon\,\omega_1}{\omega^2}\right)}{\omega^2\left(1 + \dfrac{\mathrm{Re}_\epsilon^2\omega_1^2}{\omega^4}\right)}\left(1 - \frac{\omega_1^2}{\omega^2}\right) f_\mathrm{p}^\star\,\mathcal{F}(k^\star)(\omega)\,, \tag{51}$$

with $\boldsymbol{\omega} = \begin{bmatrix}\omega_1 & \omega_2 & \omega_3\end{bmatrix}^\mathrm{T}$ the vector of angular frequencies, and with $\omega = \|\boldsymbol{\omega}\|$. The inverse Fourier transform of Eq. (51) is far from trivial, however its derivation is greatly simplified if one only wants to recover the value of $u_\mathrm{f}^\star$ at the origin of the domain (*i.e.* the centre of the particle). It reads as

$$u_\mathrm{f}^\star(\mathbf{0}) = \frac{\mathrm{Re}_\epsilon\,f_\mathrm{p}^\star}{\sqrt{2\pi}}\int_0^\infty\!\!\int_0^\pi \frac{\mathcal{F}(k^\star)(\omega)\,\sin^3(\theta)}{\left(1 + \dfrac{\mathrm{Re}_\epsilon^2}{\omega^2}\cos^2(\theta)\right)}\,\mathrm{d}\theta\,\mathrm{d}\omega\,. \tag{52}$$

If k is the Wendland kernel and $\epsilon = \delta$, or the Gaussian kernel and $\epsilon = \sigma\sqrt{9\pi/2}$, then this also reads as

$$u_\mathrm{f}(\mathbf{0}) = u_\mathrm{f,Stk}(\mathbf{0})\,\Psi_\mathrm{Os}(\mathrm{Re}_\epsilon)\,, \tag{53}$$

where $u_{\mathrm{f,Stk}}(\mathbf{0})$ is given by Eqs. (29) and (30), and Ψ_{Os} is given by

$$\Psi_{\mathrm{Os}}(\mathrm{Re}_\epsilon) = \sqrt{2\pi} \int_0^\infty \int_0^\pi \frac{\mathcal{F}(k^\star)(\omega)\, \sin^3(\theta)}{\left(1 + \dfrac{\mathrm{Re}_\epsilon^2}{\omega^2} \cos^2(\theta)\right)} \,\mathrm{d}\theta \,\mathrm{d}\omega \,. \tag{54}$$

Although the Fourier transform of the Wendland kernel is well defined, and can be shown to converge towards the Fourier transform of the Gaussian when the order of the Wendland kernel is increased [31,32], the Risch algorithm fails to find a trivial solution for the integral in Eq. (54) when k is the Wendland kernel defined in Eq. (12) with $\epsilon = \delta$. When k is the Gaussian kernel with $\epsilon = \sigma\sqrt{9\pi/2}$, however, then an expression for the Oseen correction factor can be derived and reads

$$\Psi_{\mathrm{Os}}(\mathrm{Re}_\sigma) = \sqrt{2\pi} \int_0^\infty \int_0^\pi \frac{1}{(2\pi)^{3/2}} \frac{\exp\left(\dfrac{-\omega^2}{9\pi}\right) \sin^3(\theta)}{\left(1 + \dfrac{9\pi\, \mathrm{Re}_\sigma^2}{2\,\omega^2} \cos^2(\theta)\right)} \,\mathrm{d}\theta \,\mathrm{d}\omega \tag{55a}$$

$$= \frac{3}{2\sqrt{2\pi}} \int_0^\infty \int_0^\pi \frac{\exp\left(\dfrac{-\zeta^2}{2}\right) \sin^3(\theta)}{\left(1 + \dfrac{\mathrm{Re}_\sigma^2}{\zeta^2} \cos^2(\theta)\right)} \,\mathrm{d}\theta \,\mathrm{d}\zeta \qquad \left(\text{variable change } \zeta = \omega\sqrt{2/9\pi}\right) \tag{55b}$$

$$= \frac{3}{\mathrm{Re}_\sigma^3} \left(\sqrt{\pi/2} \left(1 - \mathrm{erfc}\left(\mathrm{Re}_\sigma/\sqrt{2}\right) \exp\left(\mathrm{Re}_\sigma^2/2\right)\right) - \mathrm{Re}_\sigma + \sqrt{\pi/8}\, \mathrm{Re}_\sigma^2 \right) , \tag{55c}$$

as shown by Balachandar et al. [14]. Although not exact, an approximation of the equivalent correction factor for the Wendland kernel, when $\delta = \sigma\sqrt{9\pi/2}$, is given by

$$\Psi_{\mathrm{Os}}(\mathrm{Re}_\delta) \simeq \frac{9\pi}{4\mathrm{Re}_\delta^3} \left(9\pi \left(1 - \mathrm{erfc}\left(\mathrm{Re}_\delta/3\sqrt{\pi}\right) \exp\left(\mathrm{Re}_\delta^2/9\pi\right)\right) - 6\,\mathrm{Re}_\delta + \mathrm{Re}_\delta^2 \right) . \tag{56}$$

When $\mathrm{Re}_\delta \to 0$, it follows that $\Psi_{\mathrm{Os}} \sim 1$, while for $\mathrm{Re}_\delta \to \infty$, $\Psi_{\mathrm{Os}} \sim 9\pi/4\mathrm{Re}_\delta$. This means that for small Reynolds numbers, the Stokes flow correction will be applied, while it will be scaled down by a factor $9\pi/4\mathrm{Re}_\delta$ as the Reynolds number increases. Note that from the point of view of the numerical implementation, care must be taken as to avoid floating point errors when calculating Ψ_{Os} for small and large Reynolds numbers. Indeed, for Re_δ as large as 50, one already has $\mathrm{erfc}\left(\mathrm{Re}_\delta/3\sqrt{\pi}\right) \sim O(10^{-40})$ and $\exp\left(\mathrm{Re}_\delta^2/9\pi\right) \sim O(10^{38})$. We propose the following robust piecewise approximation of Ψ_{Os}, derived from the asymptotic series of the error function:

$$\Psi_{\mathrm{Os}}(\mathrm{Re}_\delta) = \begin{cases} 1 - \left(\dfrac{\mathrm{Re}_\delta}{8} - \dfrac{2\mathrm{Re}_\delta^2}{45\pi} + \dfrac{\mathrm{Re}_\delta^3}{216\pi} \right) + O(\mathrm{Re}_\delta^4) & \text{if } \mathrm{Re}_\delta < 0.1 \\ \dfrac{9\pi}{4} \left(\dfrac{1}{\mathrm{Re}_\delta} - \dfrac{6}{\mathrm{Re}_\delta^2} + \dfrac{9\pi}{\mathrm{Re}_\delta^3} - \dfrac{27\pi}{\mathrm{Re}_\delta^4} \right) + O(\mathrm{Re}_\delta^{-5}) & \text{if } \mathrm{Re}_\delta > 25 \\ \dfrac{9\pi}{4\mathrm{Re}_\delta^3} \left(9\pi \left(1 - \mathrm{erfc}\left(\mathrm{Re}_\delta/3\sqrt{\pi}\right) \exp\left(\mathrm{Re}_\delta^2/9\pi\right)\right) - 6\,\mathrm{Re}_\delta + \mathrm{Re}_\delta^2\right) & \text{otherwise} \end{cases} . \tag{57}$$

The correction factor Ψ_{Os} is illustrated in Fig. 8. Note that two approximations have been made to obtain the correction factor given in Eq. (56). Firstly, it corrects for the point-wise velocity interpolated to the centre of the particle, and is therefore only a first-order approximation of the similar correction for the averaged velocity. Secondly, although the Wendland regularisation kernel is considered the kernel of choice throughout this paper, the expression in Eq. (56) is, for practical reasons, derived using the "equivalent" Gaussian kernel (this approximation relies on the close qualitative similarity between the Wendland and Gaussian kernels when $\delta = \sigma\sqrt{9\pi/2}$, as shown in Section 3).

4.6. Recovery of the undisturbed flow velocity in the general case

Combining the integral Stokes flow correction derived in Section 4.2 and the Oseen correction factor derived in Section 4.5, an approximation of the averaged undisturbed flow velocity at the location of the particle, for all Reynolds numbers, is obtained from

$$\mathcal{A}(\tilde{\mathbf{u}}_\mathrm{f})_{@\mathrm{p}} = \mathcal{A}(\mathbf{u}_\mathrm{f})_{@\mathrm{p}} - \frac{\Psi_{\mathrm{Os}}(\mathrm{Re}_\delta)\, \Psi_{\mathrm{Stk}}(\lambda/\delta)\, \mathbf{f}_\mathrm{p}}{2\,\pi\,\mu_\mathrm{f}\,\delta} . \tag{58}$$

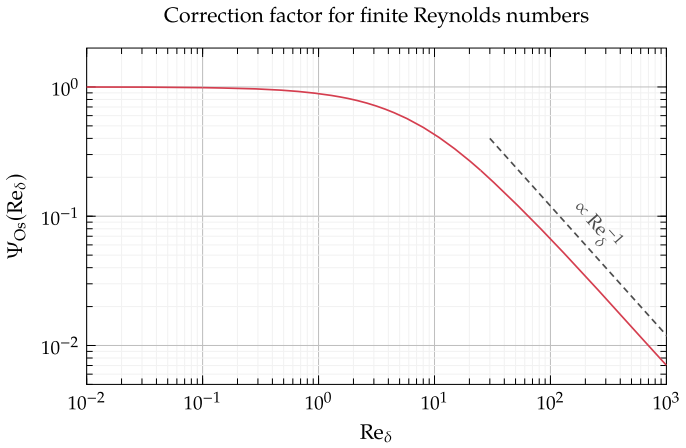

Fig. 8. Correction factor for finite Reynolds numbers, based on Oseen's approximation of the Navier-Stokes equations. The function tends to 1 for $Re_\delta \to 0$, and decays to 0 proportionally to Re_δ as the Reynolds number increases.

4.7. Application to a particle settling under the influence of gravity

The general averaged velocity correction, given in Eq. (58), is applied to a particle that is settling in a quiescent fluid under the influence of gravity. A flow domain identical to that of Section 4.4 is employed, and the flow and fluid properties are chosen as to obtain particle Reynolds numbers of $Re_p = \{0.01, 1, 100\}$ at terminal velocity.[2] The radius of the support of the regularisation kernel is chosen as

$$\delta = \max(r_p/\hat{r}_p, h/2)\,, \tag{59}$$

with $\hat{r}_p \in \{1/2, 1/3, 1/4\}$, and the radius of the support of the velocity averaging kernel is chosen as

$$\lambda = \max(\delta, 2h)\,. \tag{60}$$

The local mesh-spacing h is varied to yield particle-size/mesh-spacing ratios between $d_p/h = 0.01$ and $d_p/h = 5$. Numerically, the particle is advanced using Verlet integration [35]. The simulated particle velocities, normalised by the terminal velocity, are shown in Figs. 9, 10, and 11, as a function of the time t normalised by the particle response time

$$\tau_p = \frac{\rho_p\, d_p^2}{18\,\mu_f\, f_D}\,, \tag{61}$$

where the particle drag function is defined as

$$f_D = \frac{C_D\, Re_p}{24}\,. \tag{62}$$

The colours of the lines in Figs. 9, 10, and 11 correspond to the values of d_p/h, and each figure corresponds to a given value of $\hat{r}_p$, *i.e.* a different radius of the source term regularisation support. When no correction is employed, the terminal velocity of the particle tends to be overestimated as d_p/h increases, as is classically observed [12–14,19,22]. The larger $\hat{r}_p$, *i.e.* the smaller δ/r_p, the larger this error is. Relative errors as high as $\sim 100\%$ can be reached for $\delta/r_p = 2$, at $Re_p = 0.01$, if the averaged flow velocity is not corrected before calculating drag, as can be seen in Fig. 9. Moreover, we observe that these relative errors decrease as the particle Reynolds number increases, as is also observed in previous work [13,14]. This relates to the Oseen factor Ψ_{Os} derived in Section 4.5 converging towards zero as $Re_p \to \infty$.

Using the correction defined in Eq. (58), however, all plots qualitatively collapse on one another, with a maximum relative terminal velocity error, for all Reynolds numbers considered, that is always smaller than 10% when $\delta/r_p = 4$, as can be seen in Fig. 11. The largest errors obtained with the corrected averaged velocity are observed for values of $d_p \sim h$, which concurs with the results of the convergence study conducted in Section 4.4.

[2] Note that, although our velocity correction is shown to perform well for this range of particle Reynolds numbers, the use of the Euler-Lagrange method for $Re_p \gtrsim 100$ may be questionable, due to unresolved vortex shedding in the wake of the particle.

5. Summary

This paper provides a framework to conduct two-way coupled Euler-Lagrange simulations of dilute particle-laden flows with Lagrangian particles that can be arbitrarily large compared to the Eulerian mesh cells. They key features of this framework are summarised hereafter:

Source term regularisation The momentum transfer from the Lagrangian particles to the Eulerian fluid is enforced via a regularised momentum source term $\mathbf{M}$ given by

$$\mathbf{M} = -\sum_{\mathrm{p}} w_\delta(\|\mathbf{x}-\mathbf{x}_\mathrm{p}\|)\,\mathbf{f}_{\mathrm{p,fluid}}\,, \tag{63}$$

where $\sum_\mathrm{p}$ corresponds to the summation over all Lagrangian particles, $\mathbf{x}_\mathrm{p}$ is the centre of particle p, $\mathbf{f}_{\mathrm{p,fluid}}$ corresponds to the fluid forces acting on particle p, and w_δ is the Wendland regularisation kernel defined as

$$w_\delta(r) = \frac{21}{2\pi\delta^3}\begin{cases}(4r/\delta+1)\,(1-r/\delta)^4 & \text{if} \quad 0\le r\le\delta\\ 0 & \text{if} \quad r>\delta\end{cases}\,, \tag{64}$$

meaning that δ is the radius of the source term regularisation support.

Averaged undisturbed velocity recovery To evaluate the drag acting on a given particle p, the locally averaged undisturbed flow velocity is required, that is the local velocity from which: (a) the scales of the flow that are smaller than the particles have been filtered out; and (b) the flow disturbance due to the presence of particle p has been subtracted. We propose to recover an approximation of this locally averaged undisturbed flow velocity, $\mathcal{A}(\tilde{\mathbf{u}}_\mathrm{f})_{@\mathrm{p}}$, using

$$\mathcal{A}(\tilde{\mathbf{u}}_\mathrm{f})_{@\mathrm{p}} = \mathcal{A}(\mathbf{u}_\mathrm{f})_{@\mathrm{p}} - \frac{\Psi_{\mathrm{Os}}(\mathrm{Re}_\delta)\,\Psi_{\mathrm{Stk}}(\lambda/\delta)\,\mathbf{f}_\mathrm{p}}{2\,\pi\,\mu_\mathrm{f}\,\delta}\,, \tag{65}$$

where:

- the locally averaged flow velocity is given by

$$\mathcal{A}(\mathbf{u}_\mathrm{f})_{@\mathrm{p}} = \int_{\mathbb{R}^3} \mathbf{u}_\mathrm{f}(\mathbf{x})\,w_\lambda(\|\mathbf{x}-\mathbf{x}_\mathrm{p}\|)\,\mathrm{d}\mathbf{x}\,, \tag{66}$$

- the Oseen correction function is given by

$$\Psi_{\mathrm{Os}}(x) = \frac{9\pi}{4x^3}\left(9\pi\left(1-\mathrm{erfc}\left(x/3\sqrt{\pi}\right)\exp\left(x^2/9\pi\right)\right)-6x+x^2\right)\,, \tag{67}$$

- the Stokes correction function is given by

$$\Psi_{\mathrm{Stk}}(x) = \frac{1}{2145}\begin{cases}2145-1001\,x^2+910\,x^4-735\,x^5+250\,x^6-33\,x^7 & \text{if } 0\le x\le 1\\ 2145/x-1001/x^3+910/x^5-735/x^6+250/x^7-33/x^8 & \text{if } x>1\end{cases}\,, \tag{68}$$

and:

- $\lambda = O(r_\mathrm{p})$ is the radius of the velocity averaging operator support,
- $\mathrm{Re}_\delta = (\rho_\mathrm{f}\,\|\,\mathcal{A}(\tilde{\mathbf{u}}_\mathrm{f})_{@\mathrm{p}}-\mathbf{u}_\mathrm{p}\,\|\,\delta)/\mu_\mathrm{f}$ is the Reynolds number based on δ, the radius of the source term regularisation support.

Choice of a regularisation and averaging scale A judicious choice of the regularisation scale δ allows to match the magnitude of the flow velocity at the location of the Lagrangian particle to that of the particle velocity, when $\mathrm{Re}_\mathrm{p} \ll 1$. Notable values of δ are:

- $\delta = 3\,r_\mathrm{p}$, in which case the flow velocity at the centre of the particle is equal to the particle velocity.
- $\delta = 1536\,r_\mathrm{p}/715$, in which case the averaged flow velocity at the centre of the particle is equal to the particle velocity.
- $\delta = 2.454\,r_\mathrm{p}$, in which case the streamlines of the velocity field, for the flow through the regularised momentum source, closely match those of the Stokes flow around the spherical particle.

For simulations that aim to study the energy budget of dilute particle-laden flows, for instance, the regularisation scale $\delta = 1536\,r_\mathrm{p}/715$ and velocity averaging scale $\lambda = \delta$ are most relevant, since they allow for a consistent energy balance between the Eulerian fluid and the Lagrangian particles, in the Stokes regime (see Appendix B). In cases where the focus is to reproduce the small-scale motions of the flow as faithfully as possible, a regularisation scale $\delta = 2.454\,r_\mathrm{p}$ and velocity averaging scale $\lambda = \delta$ are more appropriate.

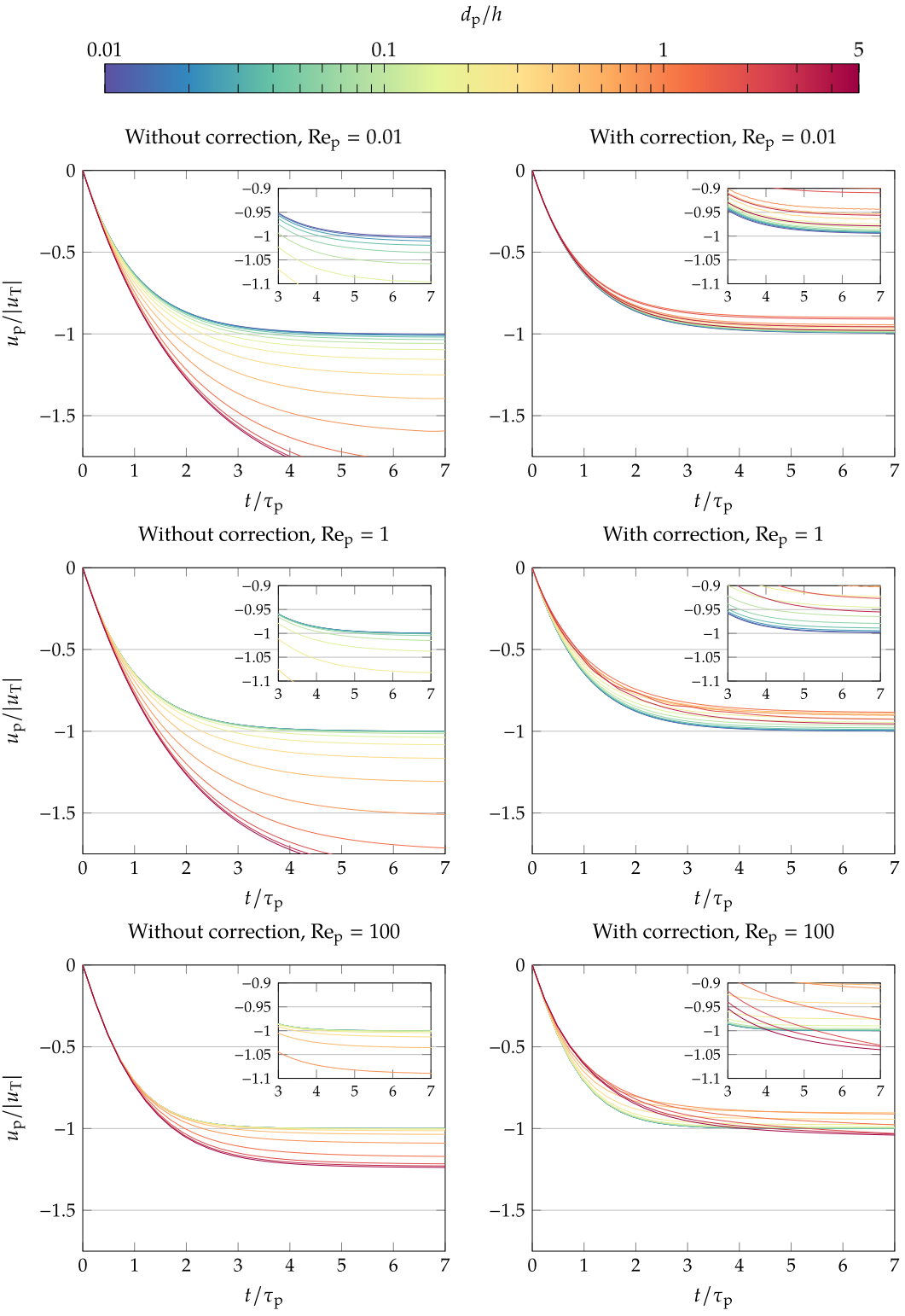

Fig. 9. Velocity of a particle settling in a quiescent fluid under the influence of gravity, normalised by its theoretical terminal velocity u_T. The regularisation support radius is defined as $\delta = \max(2r_p, h/2)$. A total of 15 cases are considered in each graph, each corresponding to a value of the particle mesh-resolution (which is varied from $d_p/h = 0.01$ to $d_p/h = 5$). Left: no correction is applied, *i.e.* the average velocity is used to estimate drag; Right: correction is applied, *i.e.* the average velocity corrected based on Eq. (58) is used to estimate drag. Top row: $Re_p = 0.01$; Middle row: $Re_p = 1$; Bottom row: $Re_p = 100$.

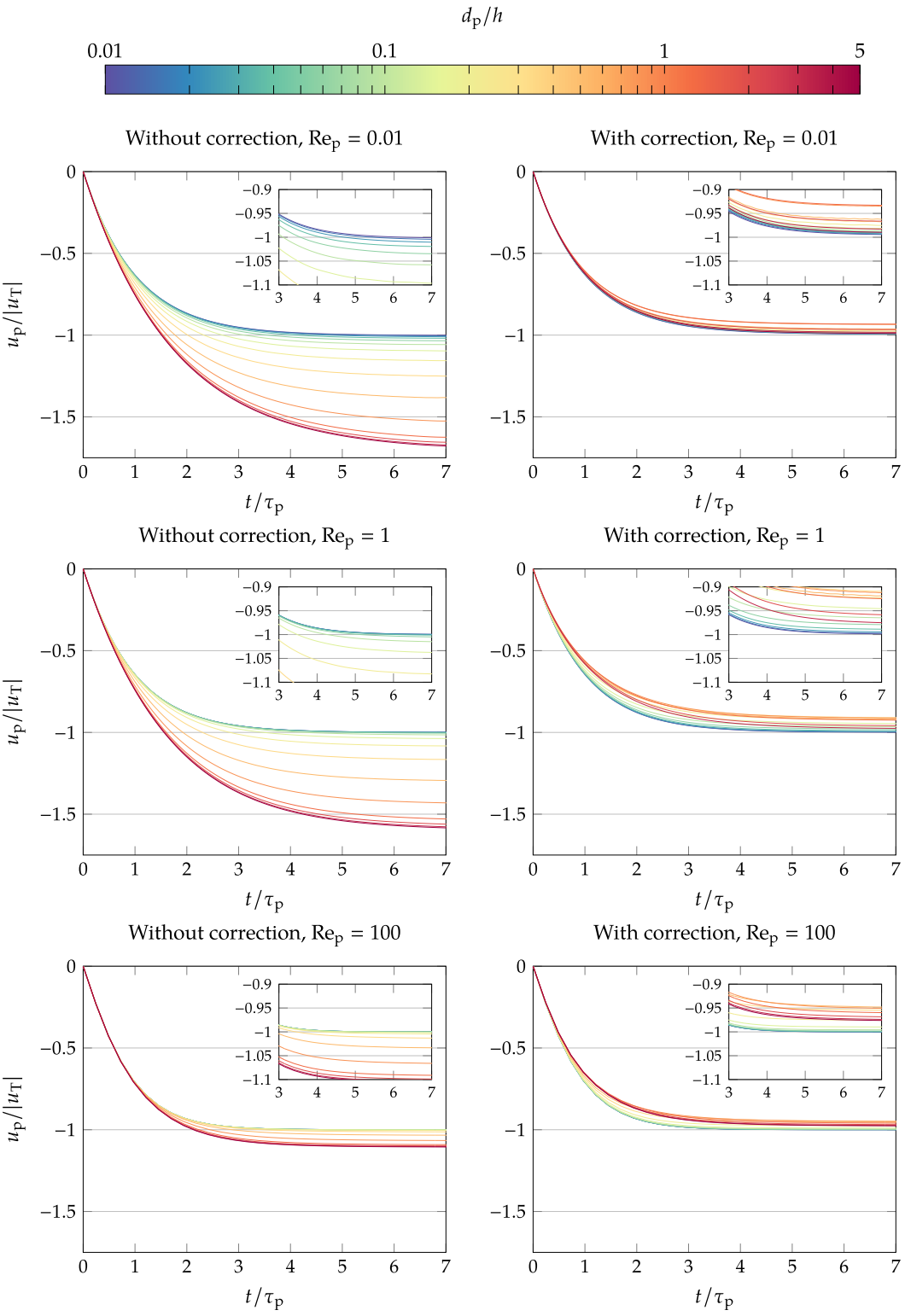

Fig. 10. Velocity of a particle settling in a quiescent fluid under the influence of gravity, normalised by its theoretical terminal velocity u_T. The regularisation support radius is defined as $\delta = \max(3r_p, h/2)$. A total of 15 cases are considered in each graph, each corresponding to a value of the particle mesh-resolution (which is varied from $d_p/h = 0.01$ to $d_p/h = 5$). Left: no correction is applied, *i.e.* the average velocity is used to estimate drag; Right: correction is applied, *i.e.* the average velocity corrected based on Eq. (58) is used to estimate drag. Top row: $Re_p = 0.01$; Middle row: $Re_p = 1$; Bottom row: $Re_p = 100$.

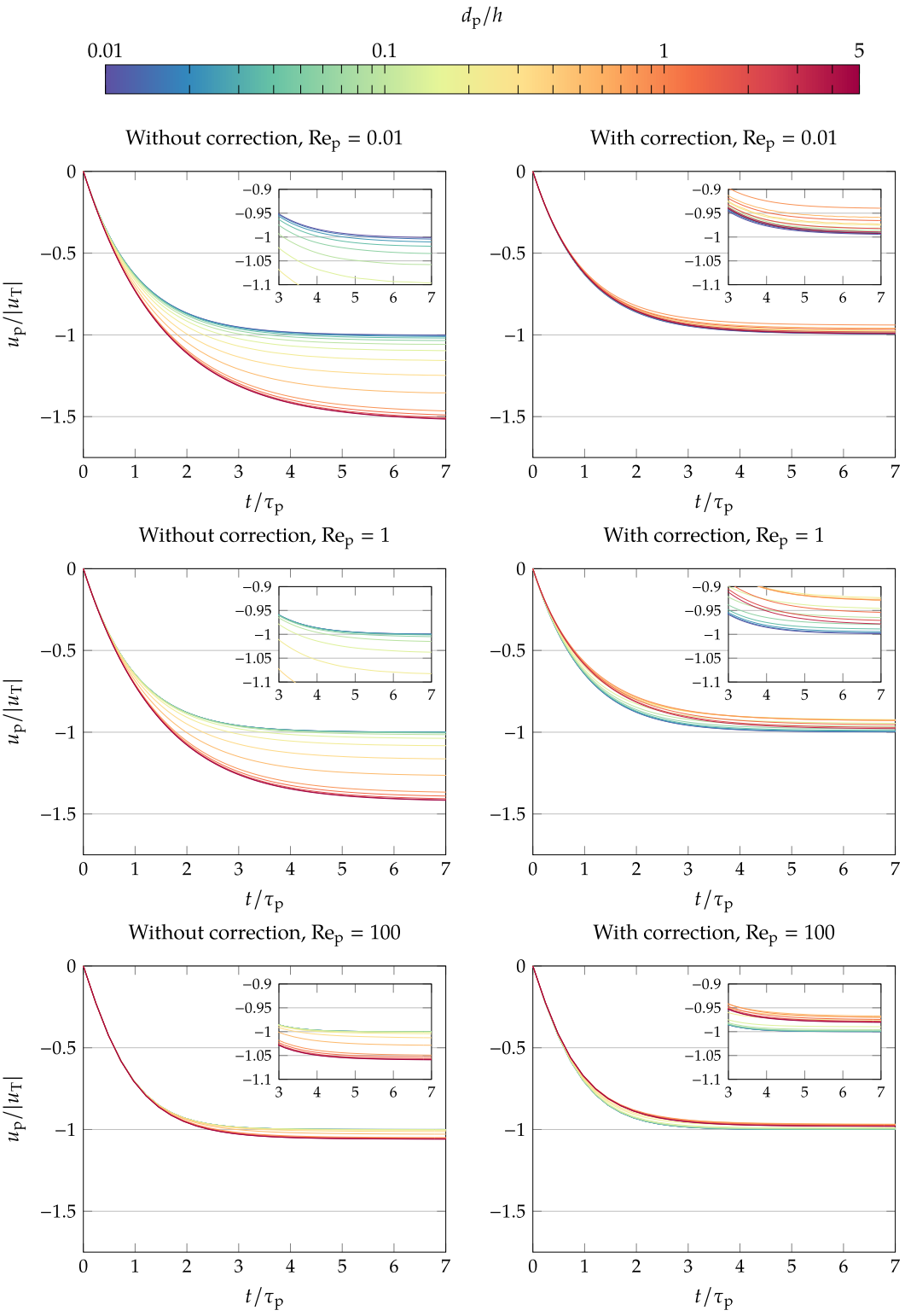

Fig. 11. Velocity of a particle settling in a quiescent fluid under the influence of gravity, normalised by its theoretical terminal velocity u_T. The regularisation support radius is defined as $\delta = \max(4r_p, h/2)$. A total of 15 cases are considered in each graph, each corresponding to a value of the particle mesh-resolution (which is varied from $d_p/h = 0.01$ to $d_p/h = 5$). Left: no correction is applied, *i.e.* the average velocity is used to estimate drag; Right: correction is applied, *i.e.* the average velocity corrected based on Eq. (58) is used to estimate drag. Top row: $Re_p = 0.01$; Middle row: $Re_p = 1$; Bottom row: $Re_p = 100$.

6. Conclusions

This paper addresses the two-way coupled Euler-Lagrange (EL) modelling of dilute particle-laden flows with arbitrary particle-size to mesh-spacing ratio. This includes particles of which the diameter can be of a similar size as, or larger than the local mesh spacing, therefore breaching the classical resolution constraint of EL methods. The approach proposed in this paper relies on the regularisation of the sources corresponding to the transfer of momentum from the Lagrangian phase to the Eulerian phase. This is achieved by convoluting these sources with a smooth regularisation kernel. Owing to the polynomial nature of the kernel function chosen in this paper, a polynomial analytical expression for the Stokes flow through the regularised momentum contribution of a particle can be derived. This, in turn, allows to exactly recover the averaged undisturbed flow velocity – a necessary quantity for the estimation of the drag acting on a finite-size particle – from the average of the local flow velocity. Based on Oseen's approximation of the Navier-Stokes equations, this correction is extended to finite values of the particle Reynolds number.

This correction is straightforward to implement in an EL numerical framework, and computationally cheap to evaluate. Moreover, it not only allows to accurately track particles that are larger than the mesh cells, but also improves the accuracy of classical PSIC-EL approaches, *i.e.* when the particles are much smaller than the computational cells. Its application to the canonical test-case of a particle settling under the influence of gravity shows that it allows to predict the terminal velocity of the particle with high accuracy regardless of the underlying mesh resolution, and that it holds over a broad range of particle Reynolds numbers. Finally, values of the regularisation scale that allow to match the local flow velocity to that of the Lagrangian particle are derived and discussed.

This approach proposed in this paper is limited to dilute particle-laden flows with particles that are away from the domain boundaries, meaning that we do not take into account the impact that neighbouring particles and/or domain boundaries can have on the flow disturbance induced by the momentum transfer.

CRediT authorship contribution statement

Fabien Evrard: Conceptualization, Formal analysis, Methodology, Software, Validation, Visualization, Writing - original draft, Writing - review & editing. **Fabian Denner:** Methodology, Resources, Software, Writing - review & editing. **Berend van Wachem:** Funding acquisition, Methodology, Resources, Software, Supervision, Writing - review & editing.

Acknowledgements

The authors are grateful to Dr. G. Zimmermann, Dr. J. Schulenburg, and Mr. D. Hasemann for their support with the HPC systems at the Otto-von-Guericke-Universität Magdeburg.

Appendix A. Regularised Stokeslet velocity with a Wendland kernel

In this appendix, we derive the expression for the regularised Stokeslet defined in Eq. (25) when the Wendland kernel is used to regularise the momentum source. To do so, we need to derive the expressions for the functions G_δ and B_δ, solutions to the equations

$$\Delta G_\delta = \Delta^2 B_\delta = w_\delta \,, \tag{A.1}$$

where w_δ is the Wendland regularisation kernel defined in Eq. (12). This task is greatly simplified by the polynomial nature of w_δ. The function G_δ is solution to the Poisson equation

$$\Delta G_\delta = \frac{1}{r^2}\frac{\partial}{\partial r}\left(r^2 G'_\delta(r)\right) = w_\delta(r) \,. \tag{A.2}$$

From the integration of the previous equation, we obtain

$$G'_\delta(r) = \frac{1}{r^2}\int_0^r s^2 w_\delta(s)\,\mathrm{d}s = \frac{1}{4\pi}\begin{cases} \dfrac{21r^6 - 90r^5\delta + 140r^4\delta^2 - 84r^3\delta^3 + 14r\delta^5}{\delta^8} & \text{if } 0 \le r \le \delta \\ \dfrac{1}{r^2} & \text{if } r > \delta \end{cases} , \tag{A.3}$$

which, integrated a second time, yields

$$G_\delta(r) = \int_0^r G'_\delta(s)\,\mathrm{d}s = \frac{1}{4\pi}\begin{cases} \dfrac{3r^7 - 15r^6\delta + 28r^5\delta^2 - 21r^4\delta^3 + 7r^2\delta^5}{\delta^8} & \text{if } 0 \le r \le \delta \\ \dfrac{3}{\delta} - \dfrac{1}{r} & \text{if } r > \delta \end{cases} . \tag{A.4}$$

The function B_δ relates to G_δ following

$$\Delta B_\delta = \frac{1}{r^2}\frac{\partial}{\partial r}\left(r^2 B'_\delta(r)\right) = G_\delta(r) \,. \tag{A.5}$$

Therefore, from the integration of this equation, we can write that

$$B'_\delta(r) = \frac{1}{r^2}\int_0^r s^2 G_\delta(s)\,\mathrm{d}s = \frac{1}{120\pi}\begin{cases} \dfrac{9r^8 - 50r^7\delta + 105r^6\delta^2 - 90r^5\delta^3 + 42r^3\delta^5}{\delta^8} & \text{if } 0 \le r \le \delta \\ \dfrac{30r^3 - 15r^2\delta + \delta^3}{r^2\delta} & \text{if } r > \delta \end{cases}. \tag{A.6}$$

The second derivative of B_δ thus reads as

$$B''_\delta(r) = \frac{1}{60\pi}\begin{cases} \dfrac{36r^7 - 175r^6\delta + 315r^5\delta^2 - 225r^4\delta^3 + 63r^2\delta^5}{\delta^8} & \text{if } 0 \le r \le \delta \\ \dfrac{15r^3 - \delta^3}{r^3\delta} & \text{if } r > \delta \end{cases}. \tag{A.7}$$

The only remaining term to determine is the constant vector $\mathbf{K}$ in Eq. (25). From the previously derived expressions for G_δ, B'_δ, and B''_δ, we know that

$$\lim_{r\to\infty} G_\delta(r) = \frac{3}{4\pi\delta}, \text{ and } \lim_{r\to\infty}\frac{B'_\delta(r)}{r} = \lim_{r\to\infty} B''_\delta(r) = \frac{1}{4\pi\delta}. \tag{A.8}$$

This means that the limit of the regularised Stokeslet velocity as $r \to \infty$ is given by

$$\lim_{r\to\infty} \mathbf{u}_\mathrm{f}(\mathbf{x}) = -\frac{\mathbf{f}_\mathrm{p}}{2\pi\,\mu_\mathrm{f}\,\delta} + \mathbf{K}. \tag{A.9}$$

The far-field value of the Stokeslet velocity is simply equal to zero, so the constant $\mathbf{K}$ is given by

$$\mathbf{K} = \frac{\mathbf{f}_\mathrm{p}}{2\pi\,\mu_\mathrm{f}\,\delta}. \tag{A.10}$$

The regularised Stokeslet velocity for the Wendland kernel therefore reads as

$$\mathbf{u}_\mathrm{f} = \frac{1}{120\,\pi\,\mu_\mathrm{f}\,\delta^8}\begin{cases} \mathbf{f}_\mathrm{p}\left(-81\,r^7 + 400\,r^6\,\delta - 735\,r^5\,\delta^2 + 540\,r^4\,\delta^3 - 168\,r^2\,\delta^5 + 60\,\delta^7\right) \\ \quad + (\mathbf{f}_\mathrm{p}\cdot\mathbf{x})\,\mathbf{x}\left(63\,r^5 - 300\,r^4\,\delta + 525\,r^3\,\delta^2 - 360\,r^2\,\delta^3 + 84\,\delta^5\right) & \text{if } 0 \le r \le \delta \\ \mathbf{f}_\mathrm{p}\left(15\,r^{-1}\,\delta^8 + r^{-3}\,\delta^{10}\right) + (\mathbf{f}_\mathrm{p}\cdot\mathbf{x})\,\mathbf{x}\left(15\,r^{-3}\,\delta^8 - 3\,r^{-5}\,\delta^{10}\right) & \text{if } r > \delta \end{cases}, \tag{A.11}$$

where $r = \|\mathbf{x}\|$.

Appendix B. Energy balance for a Lagrangian particle moving in a fluid

This appendix reproduces the derivation of the energy balance for a particle falling in fluid conducted by Maxey and Patel [23], and adapts it to the notations and characteristics of our approach. The aim is to show that, in the Stokes regime, a consistent energy balance can be established between the release of energy by the particle and the viscous dissipation in the fluid, provided that (a) the locally averaged fluid velocity is used to estimate drag, and (b) a relevant regularisation length-scale is chosen.

Consider the case of a particle moving at constant velocity in an infinitely large domain filled with quiescent fluid (this corresponds, for instance, to the equilibrium state towards which tends a particle sedimenting in fluid). We place ourselves in the Stokes regime, *i.e.* $\mathrm{Re}_\mathrm{p} \ll 1$. In the context of the two-way coupled Euler-Lagrange modelling of this particle using the approach proposed in this paper, and in the frame of reference of the particle, the momentum equation (1b) becomes

$$-\nabla p + \mu_\mathrm{f}\,\Delta\mathbf{u}_\mathrm{f} - k(\|\mathbf{x}\|)\,\mathbf{f}_{\mathrm{p,fluid}} = 0. \tag{B.1}$$

The dot product of this equation with $\mathbf{u}_\mathrm{f}$, followed by its integration over the whole domain, reads as

$$\int_{\mathbb{R}^3} -\mathbf{u}_\mathrm{f}\cdot\nabla p + \mu_\mathrm{f}\,\mathbf{u}_\mathrm{f}\cdot\Delta\mathbf{u}_\mathrm{f}\,\mathrm{d}V_\mathbf{x} - \mathbf{f}_{\mathrm{p,fluid}}\cdot\int_{\mathbb{R}^3} k(\|\mathbf{x}\|)\,\mathbf{u}_\mathrm{f}\,\mathrm{d}V_\mathbf{x} = 0. \tag{B.2}$$

Using the divergence theorem, the previous equation becomes

$$\int_{\partial\mathbb{R}^3} \mathbf{u}_\mathrm{f}\cdot(-p\,\mathbf{n} + \mu_\mathrm{f}\,\mathbf{n}\cdot\nabla\mathbf{u}_\mathrm{f})\,\mathrm{d}S_\mathbf{x} - \int_{\mathbb{R}^3}\mu_\mathrm{f}\,\|\nabla\mathbf{u}_\mathrm{f}\|^2\,\mathrm{d}V_\mathbf{x} - \mathbf{f}_{\mathrm{p,fluid}}\cdot\int_{\mathbb{R}^3} k(\|\mathbf{x}\|)\,\mathbf{u}_\mathrm{f}\,\mathrm{d}V_\mathbf{x} = 0. \tag{B.3}$$

The first integral on the left-hand side of the previous equation is equal to zero, as p and $\mathbf{u}_\mathrm{f}$ are constant infinitely far from the particle. Moving back to a fixed frame of reference, the previous equation then reads as

$$\int_{\mathbb{R}^3} \mu_\mathrm{f} \|\nabla \mathbf{u}_\mathrm{f}\|^2 \, \mathrm{d}V_\mathbf{x} + \mathbf{f}_{\mathrm{p,fluid}} \cdot \mathcal{A}(\mathbf{u}_\mathrm{f})_{@\mathrm{p}} = 0\,, \tag{B.4}$$

where $\mathcal{A}$ is the averaging operator introduced in Eq. (32). With that in mind, we have shown in Section 4.3 that in the Stokes regime,

- when using the Wendland kernel to regularise the particle momentum transfer ($k = w_\delta$),
- when the length-scale of the Wendland regularisation kernel is chosen such that $\delta = 1536\, r_\mathrm{p}/715$,
- when the undisturbed average fluid velocity at the location of the particle, $\mathcal{A}\left(\tilde{\mathbf{u}}_\mathrm{f}\right)_{@\mathrm{p}}$, integrated using the same Wendland regularisation kernel and the averaging scale $\lambda = \delta$, is used to estimate drag,

then the average disturbed velocity at the location of the particle matches the velocity of the Lagrangian particle, *i.e.* $\mathcal{A}(\mathbf{u}_\mathrm{f})_{@\mathrm{p}} = \mathbf{u}_\mathrm{p}$. In such a case, Eq. (B.4) reads as

$$\int_{\mathbb{R}^3} \mu_\mathrm{f} \|\nabla \mathbf{u}_\mathrm{f}\|^2 \, \mathrm{d}V_\mathbf{x} + \mathbf{f}_{\mathrm{p,fluid}} \cdot \mathbf{u}_\mathrm{p} = 0\,. \tag{B.5}$$

The first term on the left-hand side of Eq. (B.5) corresponds to the viscous dissipation in the fluid domain, whereas the second term corresponds to the rate of transfer of energy from the particle to the fluid. Using the undisturbed averaged fluid velocity to estimate drag, when the Wendland kernel is employed and the regularisation length-scale is chosen as $\delta = 1536\, r_\mathrm{p}/715$, thus allows to have a consistent energy balance between the Eulerian fluid and the Lagrangian particle in the Stokes regime, *i.e.* the energy released by a particle in an equilibrium state corresponds exactly to the dissipation by the viscous fluid.

Declaration of competing interest

The authors declare that they have no known competing financial interests or personal relationships that could have appeared to influence the work reported in this paper.

References

[1] M.H. Abdol Azis, F. Evrard, B. van Wachem, An immersed boundary method for flows with dense particle suspensions, Acta Mech. 230 (2018) 485–515.
[2] A. Wachs, Particle-scale computational approaches to model dry and saturated granular flows of non-Brownian, non-cohesive, and non-spherical rigid bodies, Acta Mech. 230 (2019) 1919–1980.
[3] B. van Wachem, A. Almstedt, Methods for multiphase computational fluid dynamics, Chem. Eng. J. 96 (2003) 81–98.
[4] R. Fox, F. Laurent, M. Massot, Numerical simulation of spray coalescence in an Eulerian framework: direct quadrature method of moments and multi-fluid method, J. Comput. Phys. 227 (2008) 3058–3088.
[5] C. Marchioli, A. Soldati, J.G.M. Kuerten, B. Arcen, A. Taniere, G. Goldensoph, K.D. Squires, M.F. Cargnelutti, L.M. Portela, Statistics of particle dispersion in direct numerical simulations of wall-bounded turbulence: results of an international collaborative benchmark test, Int. J. Multiph. Flow 34 (2008) 879–893.
[6] J.K. Eaton, Two-way coupled turbulence simulations of gas-particle flows using point-particle tracking, Int. J. Multiph. Flow 35 (2009) 792–800.
[7] S. Balachandar, J.K. Eaton, Turbulent dispersed multiphase flow, Annu. Rev. Fluid Mech. 42 (2010) 111–133.
[8] M. Maxey, Simulation methods for particulate flows and concentrated suspensions, Annu. Rev. Fluid Mech. 49 (2017) 171–193.
[9] S. Elghobashi, On predicting particle-laden turbulent flows, Appl. Sci. Res. 52 (1994) 309–329.
[10] B. Andersson, R. Andersson, L. Håkansson, M. Mortensen, R. Sudiyo, B. van Wachem, Computational Fluid Dynamics for Engineers, 2011.
[11] S. Elghobashi, G.C. Truesdell, On the two-way interaction between homogeneous turbulence and dispersed solid particles. I: turbulence modification, Phys. Fluids A 5 (1993) 1790.
[12] P.J. Ireland, O. Desjardins, Improving particle drag predictions in Euler–Lagrange simulations with two-way coupling, J. Comput. Phys. 338 (2017) 405–430.
[13] J. Horwitz, A. Mani, Correction scheme for point-particle models applied to a nonlinear drag law in simulations of particle-fluid interaction, Int. J. Multiph. Flow 101 (2018) 74–84.
[14] S. Balachandar, K. Liu, M. Lakhote, Self-induced velocity correction for improved drag estimation in Euler–Lagrange point-particle simulations, J. Comput. Phys. 376 (2019) 160–185.
[15] C.T. Crowe, M.P. Sharma, D.E. Stock, The particle-source-in cell (PSI-CELL) model for gas-droplet flows, J. Fluids Eng. 99 (1977) 325–333.
[16] M. Boivin, O. Simonin, K.D. Squires, Direct numerical simulation of turbulence modulation by particles in isotropic turbulence, J. Fluid Mech. 375 (1998) 235–263.
[17] B. van Wachem, J. Schouten, C. van den Bleek, R. Krishna, J. Sinclair, Modeling of gas-fluidized beds with a bimodal particle mixture, AIChE J. 47 (2001) 1292–1302.
[18] J. Capecelatro, O. Desjardins, An Euler–Lagrange strategy for simulating particle-laden flows, J. Comput. Phys. 238 (2013) 1–31.
[19] F. Evrard, F. Denner, B. van Wachem, A multi-scale approach to simulate atomisation processes, Int. J. Multiph. Flow 119 (2019) 194–216.
[20] J.-F. Poustis, J.-M. Senoner, D. Zuzio, P. Villedieu, Regularization of the Lagrangian point force approximation for deterministic discrete particle simulations, Int. J. Multiph. Flow 117 (2019) 138–152.
[21] P. Gualtieri, F. Picano, G. Sardina, C.M. Casciola, Exact regularized point particle method for multiphase flows in the two-way coupling regime, J. Fluid Mech. 773 (2015) 520–561.
[22] J. Horwitz, A. Mani, Accurate calculation of Stokes drag for point–particle tracking in two-way coupled flows, J. Comput. Phys. 318 (2016) 85–109.
[23] M. Maxey, B. Patel, Localized force representations for particles sedimenting in Stokes flow, Int. J. Multiph. Flow 27 (2001) 1603–1626.
[24] M.R. Maxey, B.K. Patel, E.J. Chang, L.-P. Wang, Simulations of dispersed turbulent multiphase flow, Fluid Dyn. Res. 20 (1997) 143.

[25] G.S. Shallcross, R.O. Fox, J. Capecelatro, A volume-filtered description of compressible particle-laden flows, Int. J. Multiph. Flow (2019) 103138.
[26] M.R. Maxey, J.R.J. Riley, Equation of motion for a small rigid sphere in a nonuniform flow, Phys. Fluids 26 (1983) 883.
[27] R. Gatignol, The Faxén formulas for a rigid particle in an unsteady non-uniform Stokes-flow, J. Méc. Théor. Appl. 2 (1983) 143–160.
[28] L. Schiller, A. Naumann, Über die grundlegenden Berechnungen bei der Schwerkraftaufbereitung, Z. Ver. Dtsch. Ing. 77 (1933) 318–320.
[29] R. Clift, J. Grace, M. Weber, Bubbles, Drops and Particles, Academic Press, New York, 1978.
[30] Y. Ling, S. Zaleski, R. Scardovelli, Multiscale simulation of atomization with small droplets represented by a Lagrangian point-particle model, Int. J. Multiph. Flow 76 (2015) 122–143.
[31] A. Chernih, I.H. Sloan, R.S. Womersley, Wendland functions with increasing smoothness converge to a Gaussian, Adv. Comput. Math. 40 (2014) 185–200.
[32] A. Chernih, S. Hubbert, Closed form representations and properties of the generalised Wendland functions, J. Approx. Theory 177 (2014) 17–33.
[33] R. Cortez, The method of regularized Stokeslets, SIAM J. Sci. Comput. 23 (2001) 1204–1225.
[34] F. Denner, F. Evrard, B. van Wachem, Conservative finite-volume framework and pressure-based algorithm for flows of incompressible, ideal-gas and real-gas fluids at all speeds, J. Comput. Phys. 409 (2020) 109348.
[35] M.P. Allen, D.J. Tildesley, The Computer Simulation of Liquids, Vol. 42, Oxford University Press, 1989.